DEUTSCHES ELEKTRONEN-SYNCHROTRON DESY

DESY 83-059
July 1983

SUMMARY

OF THE EXPERIMENTAL DISCUSSION SESSION+)

by

H. Spitzer
Universität Hamburg
Notkestr. 85
2000 Hamburg - 52

ISSN 0418-9833

+)Invited talk given at the 5th International Workshop on Photon-Photon Collisions, Aachen, April 13-16, 1983.

NOTKESTRASSE 85 · 2 HAMBURG 52

To be sure that your preprints are promptly included in the
HIGH ENERGY PHYSICS INDEX ,
send them to the following address (if possible by air mail) :

DESY
Bibliothek
Notkestrasse 85
2 Hamburg 52
Germany

DESY 83-059
July 1983

SUMMARY
OF THE EXPERIMENTAL DISCUSSION SESSION

H. Spitzer

Universität Hamburg
Notkestr. 85
D 2000 Hamburg - 52

Abstract A total of 26 papers have been contributed to the experimental discussion session. I will discuss some of the tools needed for 2γ experimentation and then point to highlights and regions of particular progress in the last two years. The process $\gamma\gamma \to \eta \to \gamma\gamma$ has been measured for the first time as well as the cross section for $\gamma\gamma \to \rho^+\rho^-$. The latter rules out a resonance interpretation for $\sigma(\gamma\gamma \to \rho^0\rho^0)$. Progress has been made in understanding the f^0 shape by an interference mechanism. Previous determinations of σ_{tot} ($\gamma\gamma \to$ hadrons) have suffered from limited detector acceptance. The ongoing analyses of PLUTO, JADE and PEP4 + PEP9 data look promising. A separation of σ_{TT} and σ_{TL} seems possible. The first measurement of the Q^2 dependence of high p_T jet production was presented. Both high p_T and high Q^2 help in extracting the Born process $\gamma\gamma \to q\bar{q}$ by suppressing competing processes. Progress has been made in measuring the photon structure function F_2. The data available have increased from the original 110 PLUTO events in 1981 to well above 2000 events from five experiments. The Q^2 limit accessible has grown from 15 GeV^2 to about 200 GeV^2. A proper unfolding method which converts the measured event distribution into a structure function $F_2(x, Q^2)$ has been presented.

1. Introduction

Two years ago at the Paris International Colloquium on Photon-Photon Interactions seven papers were contributed to the experimental discussion session. We had reports on η', f^0 and $A_2{}^0$ production and first qualitative results on the total $\gamma\gamma$ cross section, on high p_T jets and the photon structure function. This year 26 speakers presented their data. The field has grown both in quality and quantity. Table 1 gives a summary of the topics covered. Most of the data and analyses have

Table 1 Contributions to the experimental discussion session

field	speaker	topic
resonance production	A. Weinstein (Crystal Ball)	$\gamma\gamma \to \eta$
	R. Mir (TASSO)	$\gamma\gamma \to \eta'$
	M. Zachara (PLUTO)	$\gamma\gamma \to \eta'$
		$\gamma\gamma \to f^0$
	F. Kovacz (CELLO)	$\gamma\gamma \to f^0$
	J. Olsson (JADE)	$\gamma\gamma \to A_2$
	L. Köpke (TASSO)	$\gamma\gamma \to f'$
	U. Karshon (TASSO)	$\gamma\gamma \to \iota/\theta/\eta_c$ limits
exclusive processes	C. Williams (PEP9)	$\gamma\gamma \to \mu^+\mu^-$
	R. Kellogg (PLUTO)	$\gamma\gamma \to h^+h^-$
	H. Kueck (TASSO)	$\gamma\gamma \to p\bar{p}$
	M. Wollstadt (TASSO)	$\gamma\gamma \to \pi^+\pi^+\pi^-\pi^-$
	H.J. Behrend (CELLO)	$\gamma\gamma \to \pi^+\pi^+\pi^-\pi^-$
	J. Olsson (JADE)	$\gamma\gamma \to \rho^+\rho^-$
	A. Shapira (TASSO)	$\gamma\gamma \to \rho^0\rho^0$ analysis method
σ_{tot}	N. Wermes (SLAC)	problems in σ_{tot} determination
high p_T processes	E. Duchovny (TASSO)	high p_T inclusive
	H. Lierl (CELLO)	high p_T incl./jets
	S. Cartwright (PLUTO)	high p_T jets
structure functions	F. Kirschfink (TASSO)	F_2, endcap tag
	G. Carnesecchi (CELLO)	F_2, endcap tag
	T. Nozaki (JADE)	F_2, EC + barrel tag
	G. Knies (PLUTO)	F_2, endcap tag
	B. King (PLUTO)	F_2, LAT tag
	F. Raupach (PLUTO)	F_2, LAT tag
	S. Maxfield (PLUTO)	F_2, double tag
	V. Blobel (PLUTO)	unfolding methods
other	D. Miller (U. C. London)	tagging at LEP

been shown at this conference for the first time.

Faced with the task of summarizing the discussion session I realized that J. Olsson, N. Wermes, H. Kolanoski, W. Wagner and M. Pohl have given excellent summaries of the experimental results contributed to this conference. Instead of repetition I decided to concentrate rather on the status and future potential of 2γ experiments and to present a few highlights which illustrate the experimental progress we have made in the last two years. The presentation will follow the list of topics given in table 1.

For more detailed information on the 26 contributions I refer the reader to the abstracts, which are included in the symposium proceedings, and to the authors themselves.

2. Tools for 2γ experimentation

For 2γ experimentation you need first sufficient luminosity from an e^+e^- storage ring which produces the flux of virtual colliding photons.

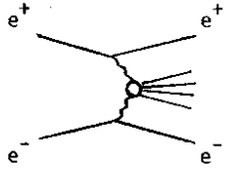

More importantly you need a detector with very good particle acceptance in both the central and forward regions. Finally 2γ experiments are not easy to analyze. Detection efficiencies can be quite low. Particles are produced preferably near the forward direction (θ=10-20°, see fig. 10), where your detector might be insensitive. So you need a lot of skill and endurance to determine a cross section.

Table 2 shows the integrated luminosities available from detectors involved in 2γ physics measurements. As is obvious from the table most of the present data come from PETRA experiments. However this trend might reverse in the future because of a dramatic luminosity increase at PEP since the beginning of 1983. In contrast the luminosity of PETRA will be relatively low during the top search with beam energies above 20 GeV.

Fig. 1 shows the acceptance of various detectors for measuring charged hadrons (full lines) and neutral showering hadrons (dashed lines). It is mandatory to have optimum coverage since in most experiments the mass of the γγ system, $W_{\gamma\gamma}$, has to be determined from the measured hadrons. The PLUTO and PEP9 experiments are best in this respect followed by JADE, MAC, CELLO and TASSO. The endcap counters of CELLO and TASSO have been not used in the past for neutral hadron measurement.

Table 2 Luminosity taken til April 1983 by e^+e^- storage ring detectors involved in 2γ measurements.

	detector	integrated luminosity analysed(pb^{-1})	lumi taken, not analysed (pb^{-1})
multi-purpose detectors	TASSO	∿ 75	-
	JADE	∿ 75	-
	CELLO	∿ 10	-
	MARK II		∿ 50
	MAC		∿ 40 *
specialized 2γ detectors	PLUTO II	45	-
	PEP 4 + 9	3	∿ 30
calorimeters	MARK J	∿ 75	-
	Crystal Ball	3 (γγ → n)	
		21 (γγ → f)	13
		SPEAR	DORIS
present data taking rate : (June 1983)		DORIS (E_b = 5 GeV)	1 - 2 pb^{-1}/week
		PEP (E_b = 14.5 GeV)	8 pb^{-1}/week
		PETRA (E_b = 20 GeV)	0.5 - 1 pb^{-1}/week

Another requirement is a potential for tagging and Q^2 measurement of electrons scattered at moderate angles (θ<100 mrad). This is vital for analyzing the Q^2 dependence of 2γ reactions and for selecting reactions with one quasireal photon (the so called target photon) by "antitagging" on the second electron. PLUTO, PEP4/9 and JADE have used such devices extensively. CELLO, TASSO and MARK II will have them for future analyses (see table 3).

Table 3 Range of small angle tagging devices with potential for Q^2 measurement

detector	tagging range (mrad)
JADE	43 - 78
PLUTO 81/82	30 - 60, 85 - 250
PEP 4 + 9	22 - 180
MARK II	20 - 85
CELLO	50 - 90 (since 1983)
TASSO	25 - 115 (since 1983)

* A first measurement of the structure function F_2 has been shown at this conference.

Two experiments have been equipped with specialized detectors for 2γ physics. Fig. 2 shows a view of the PLUTO detector as used in 1981/82. The central PLUTO detector, which has been a well known work horse since DORIS and early PETRA times has been supplemented by two forward spectrometers. These devices consist each of a magnetic spectrometer (σ_p=0.025·p), a small angle and a large angle shower counter (SAT, LAT) and a muon detector. A similar setup is available at PEP. Fig. 3 shows a view of the PEP4 and PEP9 detectors which look like a big brother of PLUTO. The magnetic forward spectrometers cover the range 24 < θ < 180 mrad with a resolution $\sigma_p = 0.01 \cdot p$ (p in GeV). In the heart of the PEP9 setup is a small angle NaI tagger with a resolution of σ_E/E = 1 % at 14 GeV. This will allow double tagging measurements with an independent bias free determination of $W_{\gamma\gamma}$. The PEP4 and PEP9 experiments started combined data taking in early 1982. Whereas PLUTO is no longer in the beam, PEP4 and PEP9 will hopefully continue for some years.

3. Resonance production

In the last four years two photon experiments have led to a renaissance of C=+1 meson spectroscopy. The excitation of meson resonances like η, η', f^0, A_2, f' occurs with ample rate in the reaction

$$\gamma\gamma \to \text{meson},$$

where both photons are quasireal (no tag mode). The final state can be selected easily as long as all particles from the resonance decay are detected. The measurements yield the radiative decay widths Γ(M→γγ) which give us insight into the quark structure of meson resonances. In addition one can set limits on the production of exotic states like glueballs or 4 quark states.

Since particle momenta from resonance decay are low (usually below 1 GeV), one needs efficient low multiplicity triggers. The boost of the γγ system in the beam direction tends to push a sizeable fraction of the decay products out of the acceptance region of existing detectors. Table 4 lists the channels which have been studied in contributions to this conference. Charged final states can be measured with detection efficiencies between 3 and 15 %, whereas for final states involving π^0's or photons the detection efficiencies drop below 1 % (with the exception of $\gamma\gamma \to \eta \to \gamma\gamma$).

In order to illustrate the difficulties encountered in the analysis I show in fig.4(a) a typical photon energy spectrum from the decay $\eta' \to \rho\gamma$, as measured by TASSO. The average photon energy is around 200 MeV, but the measurement ends at 100 MeV. Here the photon detection has dropped to 40 % for TASSO and 65 % for JADE (see fig. 4(b)).

Table 4 Production of meson resonances and four pion final states in 2γ reactions as reported at this conference

final state	detection efficiency	detector	number of events
$\eta \to \gamma\gamma$	15 %	Crystal Ball	56 ± 12
$\eta' \to \pi^+\pi^-\gamma$	0.5 %	TASSO	∿ 210
	< 1 %	PLUTO	165
$f^0 \to \pi^+\pi^-$	14 %	CELLO	∿2000 $\pi^+\pi^-$ events
$A_2 \to \rho^\pm \pi^\mp$	∿ 1 %	JADE	200
$f^0 \to K^+K^-$	∿ 3.5 %	TASSO	∿ 100
$\to K^0K^0$	∿ 5 %		∿ 25
$\pi^+\pi^+\pi^-\pi^-$	∿ 3 %	TASSO	2400
	∿ 10 %	CELLO	850
$\pi^+\pi^-\pi^0\pi^0$	0.25-0.5 %	JADE	235

In spite of these difficulties considerable progress has been made in the analysis of resonance final states involving neutrals. The reactions $\gamma\gamma \to \eta \to \gamma\gamma$ and $\gamma\gamma \to \pi^+\pi^-\pi^0\pi^0$ have been measured for the first time. Fig. 5 shows as an example the two photon mass spectrum of the Crystal Ball group. A clear peak at the mass of the η (550) is observed, leading to a radiative width of

$$\Gamma_{\eta\gamma\gamma} = (0.56 \pm 0.09) \text{ keV}.$$

This has to be compared to the table value of $\Gamma_{\eta\gamma\gamma}$ = 0.324 ± 0.046 keV determined from a measurement at Cornell involving the Primakoff effect via $\gamma N \to \eta N$ [1]. More data on $\gamma\gamma \to \eta \to \gamma\gamma$ can be expected soon, e.g. from JADE.

One of the first resonances observed in 2γ reactions has been the f^0 meson [2]. Last year a breakthrough has been made in understanding the shape of the f^0 meson peak. Previous experiments have reported a downward shift of the mass peak from the table value of 1273 MeV by about 40 - 60 MeV [3]. G. Mennesier has recently provided a theoretical framework which explains the mass shift [4]. The model describes the production of ππ and $K\bar{K}$ pairs by real photons using an unitary and analytic coupled channel formalism. The unitary corrections (final state rescattering effects) are taken from fits to previously measured ππ and KK phase shift data. The CELLO Collaboration has applied the model successfully to their data as shown in fig. 6(a) [5]. The curve contains only the Born term for $\gamma\gamma \to \pi^+\pi^-$ and a helicity 2 f^0 amplitude both with unitary corrections. The only free parameter is $\Gamma_{f\gamma\gamma}$. The f^0 meson is assumed to have the standard mass. Fig. 6(b) illustrates how the mass shift is produced by the interference between the Born and f^0 amplitudes (curve A). If the interference did not occur the mass shift would disappear (curve B).

The PLUTO Collaboration has taken a look at the Q^2 dependence of f^0 production. The histogram in fig. 7 shows the two particle mass distribution (assuming pion masses) measured in the no tag mode ($\langle Q^2 \rangle$ = 0.007 GeV^2). The open points were taken in the single tag mode with an average Q^2 of 0.4 GeV^2. The latter event distribution was multiplied by a factor of 10. Both spectra still contain a smooth background from e^+e^- and $\mu^+\mu^-$ pairs. Whereas a clear f^0 peak is observed at $\langle Q^2 \rangle$ = 0.007 GeV^2, little is left at $\langle Q^2 \rangle$ = 0.4 GeV^2. The PLUTO Collaboration will have more results on the Q^2 dependence of f^0 and η' production in the future.

A beautiful example of 2 particle final state analysis has been presented by the TASSO Collaboration. Fig. 8 shows a three dimensional scatter plot for the reaction $\gamma\gamma \to 2$ charged particles, where both particle masses have been determined by a time of flight measurement. Apart from the dominant e^+e^-, $\mu^+\mu^-$ and $\pi^+\pi^-$ production clear enhancements from the reactions $\gamma\gamma \to f'(1515) \to K^+K^-$ and $\gamma\gamma \to p\bar{p}$ are observed.

Finally we turn to the production of 4 pion final states. The CELLO Collaboration has presented a new measurement of the cross section for the reaction $\gamma\gamma \to \pi^+\pi^+\pi^-\pi^-$. The cross section reaches values close to 200 nb around 1.6 GeV (fig. 9(a)). Slightly more than half of this cross section is made up by the subprocess $\gamma\gamma \to \rho^0\rho^0$. The full points in fig. 9(b) show respectively the new results from CELLO and TASSO.

One of the highlights of this conference has been the first measurement of the reaction

$$\gamma\gamma \to \pi^+\pi^- \pi^0\pi^0$$

as reported by J. Olsson (JADE). Here four γ's had to be measured in order to reconstruct the two π^0's. The resulting upper limits for the cross section $\sigma(\gamma\gamma \to \rho^+\rho^-)$ are shown in fig. 9(b) (open points). The $\rho^+\rho^-$ cross section is much smaller than the $\rho^0\rho^0$ cross section below 1.8 GeV. As discussed in the plenary talk of H. Kolanoski this result rules out most of the previous resonance interpretations of the peak in $\sigma(\gamma\gamma \to \rho^0\rho^0)$ near 1.6 GeV.

I cannot cover the reports on exclusive two particle final states in detail. But I would like to emphasize that two groups have exploited the potential for particle identification of their detectors resulting in measurements of the reactions $\gamma\gamma \to h^+h^-$ (PLUTO) and $\gamma\gamma \to p\bar{p}$ (TASSO). TASSO has now 10 times more events than originally presented. It is remarkable that QCD calculations for the exclusive final states give the correct order of magnitude for $W_{\gamma\gamma} > 2$ GeV and $\langle p_T \rangle \simeq 1$ GeV (talks of R. Kellogg and H. Kueck).

3. The total hadronic $\gamma\gamma$ cross section

3.1 What quantities can be measured?

The total hadronic $\gamma\gamma$ cross section is a fundamental quantity. The cross section for two real photons is thought to be dominated by hadron-like interactions. Hard scattering processes with pointlike coupling of the photon to quarks take over at high Q^2 and p_T [6].

When discussing the terms contributing to the total cross section we have to consider three cases:

a) No tag mode (both electrons at angles $\lesssim$ 25 mrad). Here one approaches a measurement of the collision of two real (transverse) photons, which is described by a single cross section term:

$$\sigma(W) = \sigma_{TT}(W)$$

b) Single tag mode (one electron scattered at angles $\gtrsim$ 25 mrad). The target photon is treated as a real photon. The other photon has finite Q^2 and hence longitudinal and transverse polarization components. The cross section can be written as a sum of two terms:

$$\sigma(Q^2,W) = \sigma_{TT}(Q^2,W) + \varepsilon\sigma_{TL}(Q^2,W),$$

where σ_{TL} describes the collision of a longitudinal (virtual) photon with a transverse target photon; ε is the polarization parameter (see below, 3.3).

c) Double tag mode (both electron at angles $\theta \gtrsim$ 25 mrad). Here five terms contribute (σ_i, τ_i). For details see e.g. the talk of W. Wagner at this conference.

A full program of total cross section measurements has the following objectives (in order of increasing complexity):

1) Measure of the Q^2 and W dependence of $\sigma_{TT} + \varepsilon\sigma_{TL}$ at finite Q^2.
2) Determine $\sigma_{TT}(W,Q^2=0)$ either by extrapolation to $Q^2=0$ or by "0^0 tagging" see below, 3.3).
3) Separate $\sigma_{TT}(Q^2,W)$ from $\sigma_{TL}(Q^2,W)$ by measurements at different values of ε.
4) Determine all σ_i's and τ_i's.

3.2 Difficulties with previous cross section determinations

So far only steps 1) and 2) have been attempted. The PLUTO Collaboration has published the Q^2 and W dependence of $\sigma_{TT} + \varepsilon\sigma_{TL}$ and an extrapolation to $Q^2 = 0$ [7].

The low energy part of this extrapolation has been debated (see e.g. the talk of H. Kolanoski at this conference). No other group has published total cross section measurements so far. N. Wermes has reanalyzed the TASSO total cross section data taken up to 1980. He concludes that "given the TASSO detector of 1980 they can't determine the W dependence of $\sigma_{\gamma\gamma}$" [8].

Why are measurements of the total cross section so difficult? I see two reasons: (a) the mismatch between the final state angular distributions and the acceptance of available detectors and (b) the lack of clearcut models for the final state particles. Model parameters have to be optimized by comparison with the data, but are sensitive to effects from limited acceptance.

In order to illustrate the first point the histogram in fig. 10 shows the polar angular distribution of final state hadrons with respect to the incoming e^+e^- axis as expected from a model, which simulates hadronic events at small Q^2 (single tagging at 30-60 mrad). The distribution is strongly peaked near the forward and backward directions. The peaking becomes less pronounced for events generated according to a point-like process $\gamma\gamma \to q\bar{q}$ with subsequent fragmentation (solid curve for $Q^2 > 1$ GeV^2). The reason is twofold: (a) the finite Q^2 of the scattered electron (corresponding to $\theta > 5$ degrees) pushes the event axis away from the extreme forward/backward region (b). Since the model used constituent quark masses (m_q = 300 MeV), the extreme forward/backward region is depopulated. A finite momentum transfer is necessary for creating the quark mass.

Cross section determinations at $Q^2 < 1$ GeV^2 have to cope with particle distributions as given by the histogram. I have therefore renormalized the scale in order to get constant particle flux per cm of abscissa. Fig. 11 shows the hadron acceptance available for total cross section measurements of different detectors using this scale. The TASSO detector as of 1980 provided less than 50 % charged particle coverage and no measurement of neutral hadrons. The average detection efficiency for the hadronic final state (given a tagged event) was about 10 %. This might explain some of the particular difficulties encountered by TASSO. The PLUTO detector as of 1979 had about 50 % coverage for charged and neutral showering hadrons.

In the single tag mode the $\gamma\gamma$ cms energy has to be reconstructed from the measured hadrons. The measured energy W_{vis} is usually smaller than the true energy W. The unfolding from W_{vis} to W becomes increasingly difficult with decreasing particle acceptance.

3.3 Future potential for σ_{tot} measurements at small Q^2

The bottom part of fig. 11 shows the particle acceptance of JADE, of the 1981/82 version of PLUTO and the PEP4 + PEP9 experiment. Clearly the acceptance has improved.

In the following I will discuss two cases:

a) Single tagging experiments ($Q^2 < 1$ GeV^2)

Here we are looking forward to analyses which exploit the improved acceptance. The dash-dotted curve in fig. 12 shows the efficiency for detecting a hadronic final state if the event was tagged at an average Q^2 of 0.6 GeV^2. The efficiency has an average of 30% as compared to 10% in the 1980 TASSO data. Below 2 GeV the efficiency drops below 20%.

The PEP4 + PEP9 experiment has also a potential for separating σ_{TT} and σ_{TL}. At finite Q^2 the total cross section is given by

$$\sigma_{\gamma\gamma}(W,Q^2) = \sigma_{TT}(W,Q^2) + \varepsilon\sigma_{LL}(W,Q^2)$$

$$\text{with} \qquad \varepsilon = \frac{2\,(1-y)}{2-2y+y^2}$$

$$y \approx 1 - \frac{E_{tag}}{E_{beam}} \quad (\text{at small } \theta_{tag})$$

Using the forward shower counters of PEP9 clean tagging down to energies E_{tag} = 3.5 GeV should be possible. With E_{beam} = 14.5 GeV one then obtains for

$$E_{tag} = 0.9\ E_{beam} \quad : y = 0.1 \text{ and } \varepsilon = 0.994$$

$$E_{tag} = 0.24\ E_{beam} \quad : y = 0.76 \text{ and } \varepsilon = 0.45.$$

At $\varepsilon = 0.45$ the contribution of σ_{LT} is suppressed by about 50 %. By combining data from different ε values a separation of σ_{TT} and σ_{TL} should be possible.

b) Double tagging experiments

When both scattered electrons are measured with sufficient accuracy the energy $W_{\gamma\gamma}$ can be determined in an unbiassed way. This is clearly an advantage. However in the double tagging mode the dominant QED processes $\gamma\gamma \to l^+l^-$ are tagged also: one either has to rely on a large QED subtraction or on particle identification (lepton rejection), which again confronts one with the problem of limited acceptance.

Two groups have existing devices or future plans for double tagging. The PEP9 group will use their NaI tagging counters in the region from 24 to 90 mrad. With a measured resolution of σ_E/E = 1 % at 14.5 GeV one expects from

$$W_{\gamma\gamma} \approx 4\,(E_{beam} - E_{e1}')\,(E_{beam} - E_{e2}')$$

a resolution of

$W_{\gamma\gamma}$ (GeV)	σ ($W_{\gamma\gamma}$) (GeV)
2	0.27
4	0.25

This will be adequate for σ_{tot} determination above $W_{\gamma\gamma}$ = 2 GeV.

The ARGUS Collaboration which works at DORIS has proposed the addition of a 0^o double tagging system [9]. This system will exploit the vertical bends in DORIS close to the interaction point. Momentum degraded electrons from 2γ interactions which emerge at very small angles (between 1 and 17 mrad) will be deflected into 2 counter arrays placed close to the beampipe. Using Bismuth-Germanate (BGO) shower counters with an energy resolution of $\sigma_E/E \leq 3$ % in the energy range of E_{tag} = 3-5 GeV one expects a resolution of

$W_{\gamma\gamma}$ (GeV)	σ ($W_{\gamma\gamma}$) (GeV)
1	0.27
2	0.24
4	0.18

The question of backgrounds is not yet fully settled.

4. High p_T processes

We now turn to processes where one particle or a jet of particles is emitted at high transverse momentum(p_T) relative to the photon direction in the $\gamma\gamma$ cms. High p_T reactions have the promise of unravelling the basic process $\gamma\gamma \to q\bar{q}$ and competing hard scattering processes. Both the single particle and the jet p_T distributions from hard scattering processes like $\gamma\gamma \to q\bar{q}$ are predicted to yield the characteristic p_T^{-4} behaviour [11]. Processes where one or both of the photons interact like a ρ should give higher powers of p_T (p_T^{-6}, p_T^{-8} ...).

Data on high p_T processes first became available three years ago [12]. The inclusive single particle p_T spectra showed a hard component at large p_T ($p_T \gtrsim 2$ GeV), which could not be attributed to hadron-like $\gamma\gamma$ interactions [6), 13]. Data on jet production were encouraging but limited in statistics. At this conference a measurement of the Q^2 dependence of high p_T jet production was reported for the first time. We also have two new analyses of high p_T production in notag data.

Any analysis of high p_T jet production in $\gamma\gamma$ processes has to cope with a large background from incompletely detected annihilation events which mimic a $\gamma\gamma$ event. Table 5 shows the no tag event samples from TASSO and CELLO. After appropriate cuts the number of $\gamma\gamma$ events with $p_T^{jet} > 2$ GeV is 410 for TASSO and 60 for CELLO, but the annihilation background is of similar magnitude. It is possible to determine cross sections; but it will be difficult to analyse event shapes.

Table 5 Samples of $\gamma\gamma$ events with $p_T^{jet} > 2$ GeV presented at this conference. The TASSO analysis uses charged particles only for computing W_{vis}. Their limit at 6.8 GeV corresponds to the 10 GeV limit of CELLO.

	TASSO no tag	CELLO no tag	PLUTO single tag
W_{vis} (GeV)	3.4 - 6.8	4 - 10	4 - 13
background in final event sample	~ 40 %	51 %	3 %
events after bkd subtraction	~ 410	~ 60	181

The PLUTO group has avoided this problem by using single tag data only. The track chambers in front of the LAT help in reducing the annihilation background by a factor of 10 (by requiring p > 3 GeV and the correct sign for the electron track). Similar reductions are obtained for the SAT tag data. Table 6 shows the resulting event samples for $4 < W_{vis} < 13$ GeV before p_T cuts. The remaining backgrounds are on the 3% level. Above W = 10 GeV annihilation events with hard photon radiation become an increasingly important source of background in the tagged data sample.

Table 6 PLUTO event samples used for the high p_T analysis (before p_T cuts). Cuts: $4 < W_{vis} < 13$ GeV, $n_{ch} \geq 4$, E_{beam} = 17.5 GeV, $E_{tag} > 8$ GeV.

tagging device	SAT	LAT
Q^2 range (GeV^2)	0.1 - 1	1 - 18
$\int Ldt\,(pb^{-1})$	28	39
events observed	918	491
backgrounds:		
$\gamma\gamma \to \tau\tau$	12	20
$e^+e^- \to$ hadrons	9	5
beamgas	~1	~2
$e^+e^- \to \tau\tau$ inelastic Compton	} negligible	negligible
events after bkd subtraction	869	464

As a next step a jet analysis has been performed by determining the thrust axis in the hadronic c.m.s. Particles detected in the forward spectrometers of PLUTO have been included. Fig. 13 shows the event distribution as a function of the p_T^2 value of the thrust axis for (a) SAT tags and (b) LAT tags. The full curve is from a Monte Carlo program [14] for the process $\gamma\gamma \to q\bar{q}$ with subsequent fragmentation [15]. The dashed curve is from a generalized vector dominance model for hadron production. The data show an excess over the $\gamma\gamma \to q\bar{q}$ model, which decreases with increasing p_T and increasing Q^2. This is seen more clearly in fig. 14, where the ratio

$$\tilde{R}_{\gamma\gamma} = \frac{d\sigma/dt\ (\gamma\gamma \to \text{jets})}{d\sigma/dt\ (\gamma\gamma \to q\bar{q})}$$

is plotted as a function of p_T^{jet}. The dashed line at $\tilde{R}_{\gamma\gamma} = 1$ corresponds to production via $\gamma\gamma \to q\bar{q}$ only. Whereas the SAT data (fig. 14(a)) approach $\tilde{R}_{\gamma\gamma} \approx 1$ only for $p_T > 3$ GeV, the LAT data (fig. 14 (b)) level off at $\tilde{R}_{\gamma\gamma} \approx 1.5$ already between 0 and 3 GeV. This value of $\tilde{R}_{\gamma\gamma}$ is expected if other hard processes with a p_T^{-4} behaviour (apart from $\gamma\gamma \to q\bar{q}$) are included [11].

In summary: Considerable progress has been made in extracting evidence for the process $\gamma\gamma \to q\bar{q}$ by Q^2 suppression of competing processes. There is no need for a sizeable p_T^{-6} or p_T^{-8} component for $Q^2 > 5$ GeV^2 (fig. 14 (b)). It will be a challenge to study the jet topology in more detail by looking for the predicted 3- and 4-jet events [11].

5. Photon structure function

5.1 Introduction

Two photon reactions give access to deep inelastic electron photon scattering via

$$e\gamma \to eX.$$

Here one of the electrons is scattered at high Q^2, whereas the other one is the source of a quasireal photon (4 momentum squared $P^2 \approx 0$). The structure of the low P^2 photon is probed by the high Q^2 electron. The double differential cross section for this reaction is given by standard factors from QED and by the structure function $F_2^\gamma(x,Q^2)$ of the photon

$$\frac{d\sigma}{dxdy} \sim F_2^\gamma\ (x,\ Q^2),$$

where x is the Bjorken variable $x = Q^2/(Q^2 + W^2)$ and $y \approx (E_{beam} - E_{tag})/E_{beam}$. The formula holds in the limit $xy^2 \ll 1 - y$ which is valid for all data presented so far (see e.g. ref. 6a for more details on the formalism). The structure function has an intuitive meaning. In the quark model F_2^γ is proportional to the momentum weighted probability distribution $xG_{q|\gamma}(x,Q^2)$ of finding a quark with momentum fraction x inside the target photon, when the photon is probed in a deep inelastic collision.

The photon structure function can be calculated in leading and higher orders of QCD (at least in the region $0.2 \lesssim x \lesssim 0.8$) [17]. Detailed measurements of the structure function then permit tests of QCD.

Experimentally the determination of the photon structure function confronts one with two difficulties: (a) Due to the incomplete detection of the final state hadrons the measured quantities x_{vis} and W_{vis} differ from the true ones:

$$W_{vis} < W$$

$$x_{vis} > x.$$

Data from different experiments should be unfolded in x and W in order to be comparable. But unfolding has not yet been done in most cases. Note that the Q^2 of the scattered electron is measured with a resolution of 6 - 10% directly from the electron track direction and the energy deposited in the shower counters. No systematic shift of Q^2 occurs. (b) The Monte Carlo program needs to be "fine tuned" in order to perform adequate acceptance corrections. This is easier than in the case of the total cross section at low Q^2 since the detection efficiency for events with $Q^2 > 1$ GeV^2 is higher (see the full curve in fig. 12).

The first pioneering measurement of F_2^γ based on 110 events published two years ago by the PLUTO Collaboration [18]. At this conference much progress has been reported in four areas:

(a) The PLUTO Collaboration has now much improved statistics at "low" Q^2 ($\langle Q^2 \rangle = 5$ GeV^2).

(b) We have heard reports on x distributions at previously unaccessible values of Q^2 ($\langle Q^2 \rangle = 50 - 100$ GeV^2).

(c) A proper unfolding method has been presented.

(d) The first measurement of deep inelastic $\gamma\gamma$ scattering in double tagging mode has been made.

In the following I will discuss the progress in (a) - (d).

5.2. Q^2 range of different experiments

The variety of new data and the largely extended Q^2 range has become possible by exploiting systematically the barrel and endcap shower counters for the tagging of high Q^2 electrons. Fig. 15 (a) shows the tagging range accessible at PETRA. Full lines refer to endcap shower counters, dash-dotted lines to barrel counters, and the dashed line to the PLUTO LAT counter. Fig. 15 (b) gives the corresponding event numbers after background subtraction.

The CELLO Collaboration has already published their x distributions [19]. The TASSO group presented for the first time x distributions using the liquid argon endcap counters. JADE doubled the event numbers with endcap tag compared to their publication [20] and showed beautiful new data from the barrel counter at an average Q^2 of 110 GeV^2. The latter data are displayed in fig. 16 as an example. The PLUTO Collaboration has ten times more events from the LAT than 2 years ago and also a measurement in the endcap counters. Finally a first measurement of the x distribution from MAC at PEP was shown. For a complete display of the new data I refer to the talk of W. Wagner [16].

One of the corrections necessary for a comparison with QCD calculations is the target mass effect. The target photon will occasionally obtain sizeable values of P^2 unless this can be excluded by antitagging. The last column in fig. 15 (b) shows the antitagging range of the PETRA detectors. Only JADE and PLUTO have performed antitagging below 100 mrad on the data presented. As discussed by W. Wagner an uncertainty of 5% (15%) will be introduced into the α_s determination from F_2^γ if antitagging is performed only above 30 mrad (100 mrad) [16].

5.3. A procedure for unfolding $F_2^\gamma(x,Q^2)$

A complete determination of $F_2^\gamma(x,Q^2)$ requires the unfolding of the measured data for detector effects like track losses and finite resolution. A proper method of unfolding has been presented by V. Blobel at this conference [21]. In the following I will sketch this method. The objective is to determine the structure function $F_2^\gamma(x)$ averaged over a given interval of Q^2 from the measured values of W_{vis} and Q^2 of the events. The effect of detector resolution can be found by a Monte Carlo simulation of the events in the detector. The density of events in the Q^2 - W_{vis} plane for a structure function $F_2(x)$ is then given by

$$\frac{d^2N^{MC}}{dQ^2dW_{vis}} = \int R(W_{vis}, Q^2, x)\, F_2(x)\, dx, \qquad (1)$$

where $R(W_{vis}, Q^2, x)$ includes the photon flux, kinematical factors, the fragmentation model and the effect of the detector.

In the method, the structure function $F_2(x)$ is written as a linear superposition of B-spline functions $b_i(x)$,

$$F_2(x) = \Sigma\, a_i\, b_i(x) \qquad (2)$$

B-splines [22] are piecewise cubic polynomials, continuous up to the second derivative; they are non-negative, and each $b_i(x)$ is non-zero only in a small region of x. They have the property $\Sigma\, b_i(x) \equiv 1$. B-splines have been introduced because they have optimal interpolation properties.

Inserting (2) into (1), one obtains

$$\frac{d^2N^{MC}}{dQ^2dW_{vis}} = \Sigma\, a_i \left[\int R(W_{vis}, Q^2, x)\; b_i(x)\, dx \right]$$

$$= \Sigma\, a_i \left[\frac{d^2N^{MC}}{dQ^2dW_{vis}} \right]_i \qquad (3)$$

i.e. the generated distribution in the Q^2 - W_{vis} plane has been decomposed into contributions from the B-splines $b_i(x)$.

Now the coefficients a_i can be obtained by a maximum likelihood fit of (3) to the measured event distribution in the Q^2 - W_{vis} plane. Inserting the fitted coefficients a_i into (2) yields the unfolded structure function $F_2(x)$. Data points are calculated from (2) by integration over bins of x.

Due to the finite resolution of the detector, there are negative correlations between bin contents, resulting in local (bin to bin) oscillations. These oscillations can be reduced by the assumption that $F_2(x)$ is a smooth function. I.e. one assumes that $F_2(x)$ has no narrow structures. This is enforced by requiring that the "curvature" of $F_2(x)$ is small. The curvature is measured by an

integral over the square of the second derivative of $F_2(x)$,

$$\int \left[F_2''(x)\right]^2 dx = \Sigma\Sigma\, a_i\, c_{ij}\, a_j$$

For details I refer to ref. 23.

The unfolding procedure has been applied to the PLUTO LAT data. This is a sample of 1360 events in the Q^2 range $1 < Q^2 < 18$ GeV^2.
Fig. 17(a) shows the structure function F_2 as a function of x_{vis}. Fig. 17(b) shows the same data after unfolding. The unfolded $F_2(x)$ has a systematic shift to smaller x values as compared to $F_2(x_{vis})$, however, the shift and the overall difference is small. As a second result it was found that 'systematic' differences in $F_2(x)$ for different fragmentation models are on the level of 1σ of the statistical error.

The unfolding procedure has a relatively small effect for two reasons: (1) in the Q^2 range considered $F_2(x)$ has little structure. (2) The good particle acceptance of PLUTO makes smearing effects small. This is illustrated in fig. 18, which shows the ratio W_{vis}/W as determined from Monte Carlo events which were traced through the PLUTO central detector (shaded histogram) and the combination of central and forward detectors (open histogram). A clear improvement in resolving W_{vis} is observed in the 1981 version of PLUTO. The average ratios of W_{vis}/W from different detectors are listed in fig. 15(b) for comparison. What matters in unfolding is not just the average value of W_{vis}/W but also the width and shape of the distribution. As a combined measure we use the ratio of width to mean. The smaller the ratio, the better. Typical values of σ/mean are shown in table 7.

Table 7 The ratio "standard deviation σ/mean value" of the distribution of W_{vis}/W for different detectors. The last line refers to an analysis where only charge balanced events are included.

detector	mean = $\langle \frac{W_{vis}}{W} \rangle$	$\frac{\sigma}{\text{mean}}$
PLUTO 1979	~ 0.6	0.6
JADE	0.7	0.3
PLUTO 1981 LAT	0.75	0.27
EC	0.91	
PLUTO 1981 LAT $\Sigma q_i = 0$	0.90	0.18

A method for minimizing the systematic shift of W_{vis} has been presented by F. Raupach from the PLUTO collaboration. He reduced the track losses by selecting charge balanced events with $n_{ch} \geq 4$ only. As a consequence the W_{vis}/W ratio rises to 0.9 and σ/mean drops to 0.18, which makes unfolding easy. However a price is paid by loosing two thirds of the events.

In summary, unfolding the measured x_{vis} distribution can and should be done. It requires an adequate acceptance and resolution of the detector (σ/mean < 0.3) and sufficient statistics.

5.4. γγ Cross section from double tagging

First measurements of hadron production in double tag reactions were presented by the PLUTO Collaboration. The outgoing electrons were tagged by combinations of the SAT and LAT shower counters. A total of about 200 events was found after background subtraction. When restricting to LAT - SAT combinations ($\langle Q^2 \rangle$ = 6 GeV², P^2 = 0.4 GeV²) about 70 events are left. Fig. 19 shows the resulting cross section $\sigma_{\gamma\gamma} \cdot Q^2/4\pi^2\alpha^2$ as a function of x. Here x is defined by $x = Q^2/(Q^2 + p^2 + W^2)$. The dashed curve is from a VDM calculation assuming the interaction of a highly virtual photon with a target ρ meson [24]. The full curve is the sum of the VDM contribution and a quark parton model calculation. Good agreement is found.

6. Plans for Gamma - Gamma Tagging at LEP

(contributed by David J. Miller, University College London)

6.1. The Four Forward-Detectors

It was difficult to get any information from the LEP collaborations in time for the Aachen meeting. The technical proposals were still being written and some features of the detectors were not settled. Table 8 is a "snapshot" of the plans in April 1983.

For ALEPH there is a note from Heidelberg [25] which discusses the forward detector entirely in terms of luminosity monitoring. The details in the table are according to that note, but during the presentation at Aachen it was said [26] that improvements would be made to turn the forward detector into a proper tagger. For DELPHI the details given were obtained by word of mouth at Aachen [27]. For L3 the information came by telephone [28]. The OPAL design is our responsibility [29].

Table 8 Plans for LEP Forward Detectors; April 1983

	ALEPH	DELPHI	L3 small angle	L3 large angle	OPAL
θ_{min} (mr)	45	43	24	<58	45
θ_{max} (mr)	80	∿ 144 (beyond flare)	58	120	117
z front (cm from intersection)	248	233	300	150	216
Beam pipe	flared (trumpet)	flared			parallel Be
Calorimeter Technique	Pb with gas-tubes	Pb/Bi with scintillating fibres* and VPT's+	BGO with Si Photodiodes		Pb-scintillator with VPT's+ or GPD's
Longitudinal Division	Yes	No	No		Preradiator + 2 layers*
Tracking	Minidrift or drift tubes	Tube chambers	Yes		Radial drift
Spacing of chambers	over 20 cm	over 10 cm	?		2 over 40 cm + 1 after preradiator
Luminosity Monitoring					
- Fine	Chambers	Chambers	Chambers		Chambers plus counters
- Through miniβ	Yes	No	Yes		Yes

* see text
\+ VPT is vacuum phototriode, GPD is gas filled diode (under development at UCL)

Acceptance: The LEP beampipe fixes the minimum tagging radius. All but L3 have their forward detector at about 2.2 m from the intersection. L3 divides the forward detector into two parts and is able to go to smaller angles by placing the inner part of the tagger further away.

Beampipes: All except OPAL expect to use a flared beampipe. OPAL wants a parallel pipe so that the inner vertex chamber can slide over it.

Calorimetry: The DELPHI calorimeter will use Wood's metal (low melting point Pb-Bi alloy) as a dense matrix around scintillating fibres. L3 have sufficient light from BGO to be able to use silicon photodiodes. DELPHI and OPAL plan to use vacuum phototriodes or gas filled photodiodes.

Tracking: ALEPH had planned only partial ϕ coverage for their tracking chambers but may be changing to full 2π coverage. Only OPAL plans to have sufficient lever-arm to be able to project back to the crossing point with any precision.

6.2. Motivation for the OPAL Design

The OPAL forward detector is probably the most elaborate [30]. It is intended to tag electrons down to the lowest possible energy; to ∿10% of beam energy if possible. Only at low tagged energies will it be possible to resolve the contribution from the longitudinal structure function F_L to deep inelastic $e\gamma$ scattering. To recognise these low energy electrons it will be necessary to resolve their tracks clearly before the calorimeter and to reject the pion background which becomes serious at less than 40% of beam energy in the forward direction. This is why OPAL has a large space for tracking and three longitudinal subdivisions to its forward electromagnetic calorimeter.

6.3. Rates

The rates for deep inelastic $e\gamma$ scattering for a given integrated luminosity should be higher than at PETRA/PEP. As an example one expects for $E_{beam} = 50$ GeV, $20 < \theta_{tag} < 200$ mr, $5 < E_{tag} < 50$ GeV, $\int Ldt = 10\,pb^{-1}$ and full hadron acceptance about 1400 events with $Q^2 > 5\ GeV^2$ and $W^2 > 10$ GeV, as compared to 240 events at PETRA (with same cuts except $E_{beam} = 18$ GeV, $3 < E_{tag} < 18$ GeV) [31]. In summary, the prospects for 2γ physics at LEP are good.

7. Final remark

We have seen an impressive and growing variety of attempts to master the art of 2γ experimentation. The results have mainly come from PETRA. I hope that the colleagues from PEP and elsewhere will join in soon with their results.

Acknowledgement

I thank all speakers of the experimental discussion session for their cooperation. I also thank Prof. Christoph Berger, who worked hard on making this stimulating, high level conference possible. I am indebted to Prof. V. Blobel and Dr. J. Dainton for their help in preparing this manuscript.

References

1. Particle Data Group, Phys. Lett. 111B (1982)
2. PLUTO Collaboration, Ch. Berger et al., Phys. Lett 94B (1980) 254
3. S. Cooper, talk at the 2nd International Conference on Physics in Collision, Stockholm, 2. - 4. June 1982, DESY report 82-050 (1982)
4. G. Mennessier, Zeits. Phys. C16 (1983) 241
5. CELLO Collaboration, to be published and talk of F. Kovacz at this conference
6. Ch. Berger, Proc. Fourth International Colloquium on Photon-Photon Interactions, Paris, 1981, ed. G.W. London. World Scientific, Singapore (1981), D. Cords, ibidem.
7. PLUTO Collaboration, Ch. Berger et al., Phys. Lett. 99B (1981) 287
8. N. Wermes, thesis, Bonn University, report BONN-IR-82-27 (July 1982) and talk in the Experimental Discussion Session
9. ARGUS Collaboration, A proposal to study $\gamma\gamma$ interaction with the detector ARGUS at DORIS, 1983, PRC 83/06 (unpublished)
10. JADE Collaboration, Phys. Lett. 113B (1982) 190
11. S. Brodsky, T. De Grand, J. Gunion, J. Weis, Phys. Rev. D19 (1979) 1418
12. W. Wagner, Proc. XX. Intern. Conf. on High Energy Physics Madison, Wisc. 1980, ed. L. Durand and L.G. Pondrom, American Institute of Physics, New York 1981
13. N. Wermes, talk at this conference
14. J.A.M. Vermaseren, program writeup (1978), unpublished
15. The Feynman-Field option inside the Lund program was used; T. Sjostrand, Lund University, Theor. Phys. report 80-3 (1980)

16. W. Wagner, talk at this conference
17. see eg. D. Duke, W. Frazer, talks at this conference
18. PLUTO Collaboration, Ch. Berger et al., Phys. Lett. 107B (1981) 168
19. CELLO Collaboration, Phys. Lett. 118B (1982) 211 and DESY report 83-018 (1983), to be published
20. JADE Collaboration, Phys. Lett. 121B (1983) 203
21. The method has already been applied to ν structure function data in: Charm Collaboration, Phys. Lett. 102B (1981) 67 and 109B (1982) 133. See also S. Provender, Comp. Phys. Comm. 27 (1982) 213
22. C. de Boor, A practical guide to splines, New York 1978
23. V. Blobel, transparencies of talk in the experimental discussion session, unpublished
24. J. Dainton, S. Maxfield, private communication
25. "Luminosity Monitor for ALEPH", B. Falkenburg et al., Heidelberg; ALEPH Note 93, February 1983
26. Dr. Grupen, Siegen, private communication
27. Dr. Lillestøl, Bergen, private communication
28. Prof. R. Kraemer, Carnegie Mellon University
29. U. C. London, Maryland, Bolcgna
30. Technical Proposal for the OPAL Experiment, submitted to the LEP Committee at CERN, May 1983
31. M. Davier, $\gamma\gamma$ Physics at LEP, Proc. Fourth International Colloquium on Photon-Photon Interactions, Paris 1981, World Scientific, Singapore, 1981

Discussion

T. Nozaki (Lancaster)

Are there any reasons why you did not comment on the ln Q^2 dependence of F_2 which was observed in the Q^2 range from 10 - 100 GeV^2?

H. Spitzer (Hamburg)

I consider the new data on F_2 to be an important achievement. The ln Q^2 dependence of F_2 has been summarized by W. Wagner.

T. Nozaki (Lancaster)

A comment: The structure function F_2 increases by about 50 % from 10 to 100 GeV^2 of Q^2 value according to the ln (Q^2/Λ^2) prediction. On the other hand the contribution of c quark production increases the F_2 function by about 30 - 40 % for the same Q^2 range. These two factors altogether give a factor 2 increase of F_2 in this Q^2 range. This is in good agreement with the data.

N. Wermes (SLAC)

Comment concerning 1γ background in high p_t jet processes: As pointed out in the experimental parallel session by E. Duchovni the 1γ background to 2γ jet events is due to initial state radiation only in the TAG case. For NOTAG data 1γ events are accepted dominantly due to acceptance losses.

H. Spitzer (Hamburg)

My statement about the dominance of 1γ background accompanied by a hard radiation in fact referred to the TAG case. It becomes important for $W_{vis} > 10$ GeV.

N. Wermes

I personally think that the experimental situation concerning a possible measurement of 3 or more jet processes is not that hopeless. I agree with you that a positive identification of the beam pipe jet is probably very difficult if not impossible. But applying an "ANTI-BEAM-PIPE-JET"-cut, requiring no hadronic particles in forward/backward directions and comparing to present data which do not apply this cut could possibly improve our knowledge about these processes a lot. Would you like to comment on this?

H. Spitzer

This should be tried, but it will be hard. Recall that the average width of jets is expected to be large, e.g. 50 % of the energy from $e^+e^- \to q\bar{q}$ jets at $E_{cm} = 9.4$ GeV comes outside a cone of 54° full opening angle.

H. Kolanoski (Bonn)

You showed plots where the jet cross section has been described by $\gamma\gamma \to q\bar{q}$ + GVDM. What do you mean with "GVDM"?

H. Spitzer

The GVDM model of the PLUTO group assumes that the cross section has a Q^2 dependence as given by the GVDM model of Ginzburg and Serbo (Phys. Lett. 109 B (1982) 121) and a W dependence of (240 + 270/W) nb, (W in GeV). Particles are produced in two clusters along the photon direction in the $\gamma\gamma$ cms and fragmented according the Lund model.

S. Barshay (Aachen)

Is there any enhanced or resonant-like behavior in $\gamma\gamma \to \pi\pi$ in the experimental data in the mass region of 500 MeV - 1 GeV?

H. Kolanoski

There is a measurement of $\gamma\gamma \to \pi^+\pi^-$ for $m_{\pi\pi}$ from threshold to $\sim$ 0.7 GeV from DCI. They observe about twice as large a cross section as expected from the Born cross section. However, the statistical significance is only 2.3 standard deviations.

S. Barshay

The reason that this is interesting is that there are at present some small discrepancies in muonic X-rays from muons close to a nucleus. It would be nice to know whether the 2π field at low mass can connect significantly, via 2γ, with the muon.

J. Olsson (DESY)

I would like to answer concerning $\gamma\gamma \to \pi\pi$. There are limits from JADE on the product of $B_{\pi\pi} \cdot \Gamma_{\gamma\gamma}$ between 600 MeV and 1 GeV for narrow resonances ($\Gamma \leq 50$ MeV). These limits are $\sim$ 0.5 KeV. We are working on similar limits for broad resonances.

F. Kovacs (Paris VI)

Answer to S. Barshay about $\pi\pi$ events under 1 GeV/c^2 mass: We are starting an analysis at CELLO on $ee \to (ee)\ \gamma\gamma \to (ee)\ \pi\pi$ in the mass range of 500 MeV/c^2 to 1 GeV/c^2. We have there a lot of data. For the moment our problem is to subtract tails coming from inclusive events with p_t^{total} conserved like:

- $\pi\pi$ from 4π events
- $\pi\pi$ from η' (where the γ is soft)
- $\pi\pi$ from $A_2 \to \rho^{\mp}\pi^{\pm}$ (where the π^0 is hard with low p_t)
- etc.

Then, if we have an excess of events we will try to fit our data with Menessier's model which includes broad resonances in that mass region and try to do the junction with DCI results at very low W. It seems indeed of great interest to have results of $\pi\pi$ production by $\gamma\gamma$ in the low mass region.

J.H. Field (Paris VI)

Two comments on the CELLO contributions:

1. The number of $\pi\pi$ events used in the f^0 analysis for $1.0 < M_{\pi\pi} < 1.4$ GeV/c^2 was 2031 not 50 (the latter figure corresponds to $\eta' \to \pi^+\pi^-\gamma$ $\pi\pi$ production).
2. In the untagged high p_t jet analysis for a cut $p_t^{Jet} > 2$ GeV we see $\sim$ 2 times the box contribution which is not inconsistent with the PLUTO findings.

Figure captions

Fig. 1 Acceptance for measurement of charged hadrons (full line) and neutral showering hadrons (dashed line) in existing 2γ detectors at DESY and SLAC.

Fig. 2 Side view of the PLUTO detector as operated from 1981 to 1982.

Fig. 3 Side view of the PEP4 and PEP9 detectors at SLAC. The shower counters surrounding the TPC and in the forward spectrometer are shown cross-hatched.

Fig. 4 (a) Typical photon energy spectrum from resonance decay: decay $\eta \to \rho\gamma$ as measured in the TASSO experiment (talk of R.Mir). (b) Photon detection efficiencies using the barrel lead glass counter of JADE (full curve from ref. 10) and the barrel liquid argon counters of TASSO (dash-dotted curve from talk of R. Mir), respectively.

Fig. 5 Two photon mass spectrum of the reaction $\gamma\gamma \to \eta \to \gamma\gamma$ measured by the Crystal Ball detector at SPEAR. Background from cosmic rays etc. has been subtracted. The data are from a run with $\int Ldt = 2.7\ pb^{-1}$ at 2.5 GeV < E_{beam} < 3.625 GeV (from the talk of A. Weinstein).

Fig. 6 (a) Dipion mass spectrum of reaction $\gamma\gamma \to \pi^+\pi^-$ from CELLO fitted to the Menessier model (no tag data with $<Q^2>=0.0016\ GeV^2$) (b) Curve A is the prediction of the Menessier model for interference of $\gamma\gamma \to f^0 \to \pi^+\pi^-$ (helicity 2, $\Gamma_{f\gamma\gamma}$=3 keV) and an unitarized Born term amplitude. Curve B would $f_{\gamma\gamma}$ result, if the f^0 and Born amplitudes would add incoherently (from talk of F. Kovacz).

Fig. 7 Invariant two particle mass distribution (assuming pion masses) of the reaction $\gamma\gamma \to$ 2 charged particles. The data still contain the dominant background contribution from e^+e^- and $\mu^+\mu^-$ final states. Data from PLUTO taken in the no tag mode (histogram, $<Q^2>=0.007GeV^2$) and in the tag mode multiplied by a factor 10 (open points, $<Q^2>=0.4\ GeV^2$) (from the talk of M. Zachara).

Fig. 8 Scatter plot of M^2 (positive track) vs. M^2 (negative track) from the reaction $\gamma\gamma \to$ 2 charged particles, where both particle masses have been determined by a time of flight measurement. Data from TASSO as reported by L. Köpke.

Fig. 9 (a) The cross section for reaction $\gamma\gamma \to \pi^+\pi^+\pi^-\pi^-$ as measured in the no tag mode by the CELLO collaboration. (b) The cross section for $\gamma\gamma \to \rho^0\rho^0$ from TASSO and CELLO and upper limits for $\sigma(\gamma\gamma \to \rho^+\rho^-)$ from JADE. TASSO assumed isotropic production and decay of the ρ's. CELLO assumed isotropic production and decay angular distributions as determined from the data. (from the talks of H.J. Behrend, M. Wollstadt and J. Olsson).

Fig. 10 Generated polar angular distribution of charged and neutral hadrons for the process $\gamma\gamma \to$ hadrons at small Q^2 (histogram). The spectrum has been generated by a GVDM Monte Carlo program with Lund fragmentation (for details see "Discussion") for E_{beam} = 17.5 GeV and the SAT tagging range of the PLUTO detector. No detector effects are included. The curve shows a corresponding distribution for the large angle tagging range of PLUTO ($Q^2>1GeV^2$) and W>3GeV. The distribution was generated by a $\gamma\gamma \to q\bar{q}$ Monte Carlo program using constituent quark masses and Feynman-Field fragmentation.

Fig. 11 Acceptance for σ_{tot} ($\gamma\gamma \to$ hadrons) available in experiments at PETRA and PEP. The abscissa has been renormalized in order to get constant flux per cm of abscissa using the histogram of fig. 10.

Fig. 12 Detection efficiency for multihadron final states as a function of $W_{\gamma\gamma}$ (true). Full curve: PLUTO structure function analysis with a LAT tag ($<Q^2>=5GeV^2$). Dash-dotted curve: JADE total cross section analysis (in progress) with a small angle tag ($<Q^2>=0.6\ GeV^2$).

Fig. 13 The p_T^2 distribution of the thrust axis in the hadronic cms of events $\gamma\gamma \to$ hadrons from PLUTO: (a) events tagged at small Q^2, (b) events tagged at large Q^2.

Fig. 14 The ratio $\hat{R}_{\gamma\gamma}$ of the measured cross section for $\gamma\gamma \to$ hadrons and the expected cross section for $\gamma\gamma \to q\bar{q}$ (u, d, s, c quarks) plotted vs. the p_T of the thrust axis. I.e. all events are analyzed assuming a 2jet shape. Dotted line: prediction for $\sigma(\gamma\gamma \to q\bar{q})$. (Figs. 13 and 14 from the talk of S. Cartwright).

Fig. 15 (a) Tagging range accessible for measurements of the photon structure function using PETRA detectors. Full lines: endcap counters (EC), dash-dotted lines: barrel counters (BA), dashed line: PLUTO large angle tagger (LAT). (b) Numbers of deep inelastic eγ scattering events found after background subtraction. Also given is the ratio W_{vis}/W of measured and "true" energy of the hadronic final state and the potential for antitagging (vetoing) on a second scattered electron below 100 mrad.

Fig. 16 x_{vis} distribution from deep inelastic eγ scattering with an electron tagged in the barrel shower counter of JADE. The full curve is from a leading order QCD calculation for u,d,s,c quarks. Effects of the finite photon target mass are included. For details of the calculation see ref. 20 (from talk of T. Nozaki).

Fig. 17 (a) The structure function $F_2(x_{vis})/\alpha$ averaged over the range $1 < Q^2 < 18$ GeV^2 as a function of x_{vis}. Data from PLUTO. The data points still contain a background of about 12% (mostly from $\gamma\gamma \to \tau\tau$).

(b) The unfolded structure function $F_2(x)/\alpha$. The background has been subtracted in the unfolding procedure. The curves are from a quark parton model calculation for uds quarks (dash-dotted curve) and udsc quarks (full curve) using $m_u = m_d = 0.3$ GeV, $m_s = 0.5$ GeV and $m_c = 1.6$ GeV.

Fig. 18 The ratio W_{vis}/W as determined from the PLUTO central shower and track detectors (shaded histogram) and from the central and forward detectors (open histogram).

Fig. 19 The hadronic cross section $\sigma_{\gamma\gamma} Q^2/(4\pi^2\alpha^2)$ measured in the double tag mode by the PLUTO Collaboration at $\langle Q^2 \rangle = 6$ GeV^2 and $\langle P^2 \rangle = 0.4$ GeV^2. The dashed curve is from a VDM calculation assuming the interaction of a highly virtual photon with a target ρ meson. The full curve is the sum of the VDM contribution and a quark parton model calculation for u,d,s,c quarks with constituent masses.

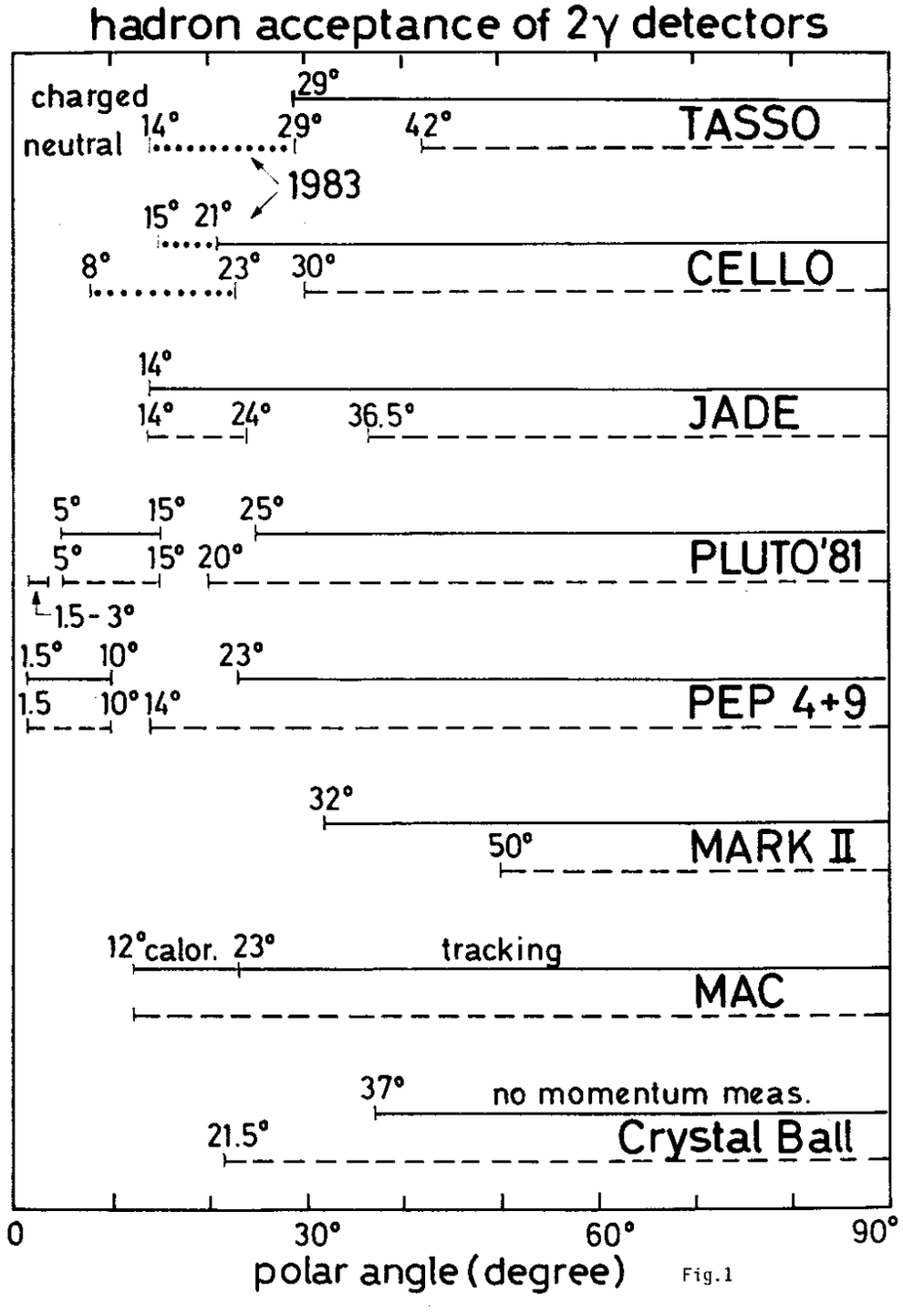

Fig.1

PLUTO Detektor (1981)

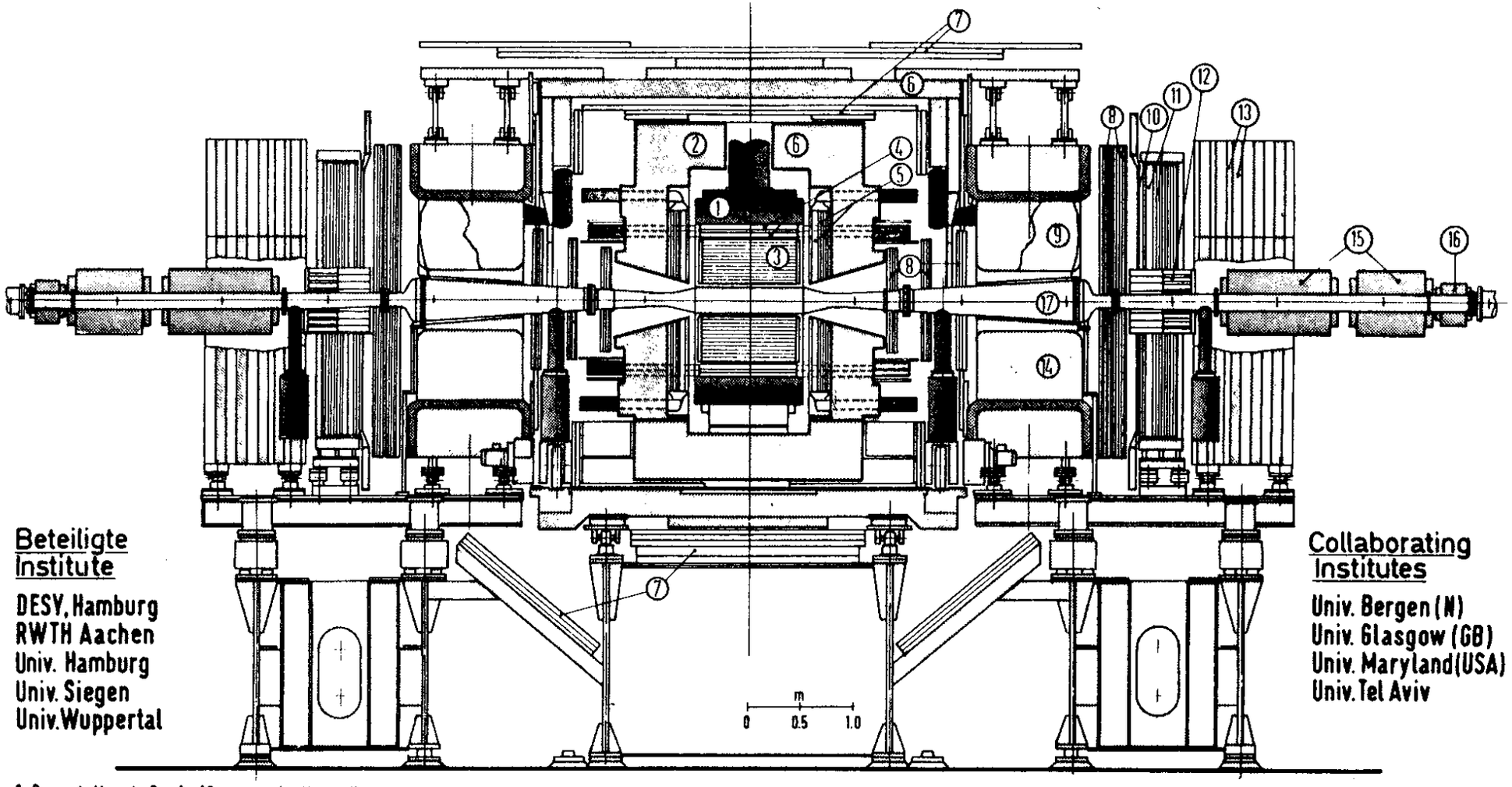

Beteiligte Institute

DESY, Hamburg
RWTH Aachen
Univ. Hamburg
Univ. Siegen
Univ. Wuppertal

Collaborating Institutes

Univ. Bergen (N)
Univ. Glasgow (GB)
Univ. Maryland (USA)
Univ. Tel Aviv

1 **Supraleitende Spule /** Superconductive coil
2 **Eisenjoch /** Magnet yoke
3 **Zylindr. Driftkammern /** Cylindr driftchambers
4 **Zylindr. Schauerzähler / mit Helix-Rohren** Barrel shower counter with helix-tubes
5 **Endkappen Schauerzähler / mit Proport. Kammern** Endcap shower counters with proportional chambers
6 **Hadron-Absorber /** Hadron absorber
7 **Myon-Kammern /** Muon chambers
8 **Vorwärts-Driftkammern /** Forward drift chambers
9 **Cerenkov Zähler /** Cerenkov counter
10 **Flugzeit-Zähler /** Time of flight counters
11 **Weitwinkel Schauerzähler / mit Proport. Kammern** Large angle tagger (LAT) with proport. tubes
12 **Bleiglaszähler Matrix /** Small angle tagger (SAT)
13 **Vorw. Myon Detektor /** Forward muon detector
14 **Septum Magnet /** Septum magnet
15 **Mini-Beta Quadrupol /** Mini beta quadrupole
16 **Korrektur Quadrupol /** correction quadrupole
17 **Vakuumkammer /** Vacuum pipe

Fig.2

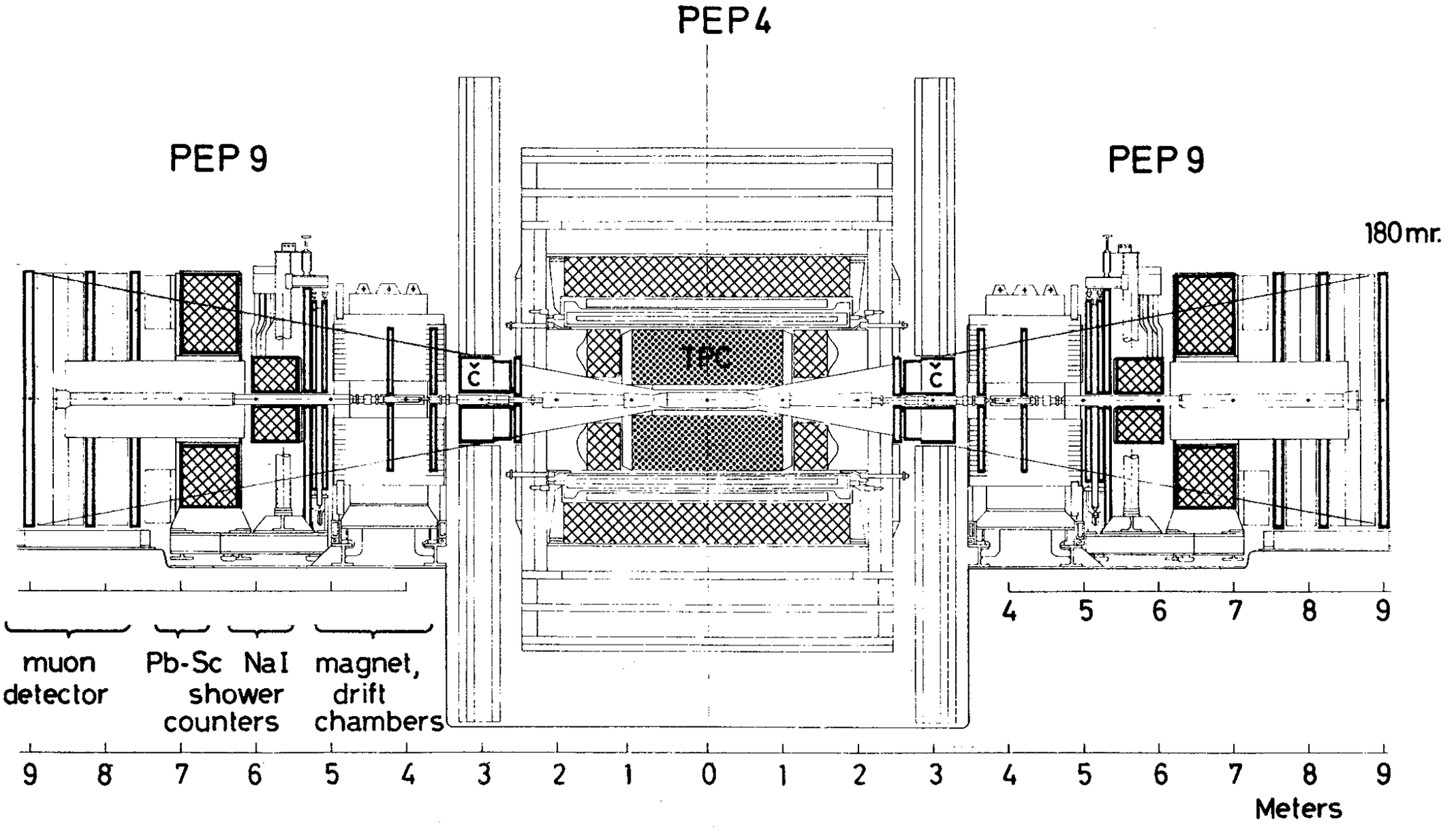
PEP4
PEP 9
PEP 9
180mr.
TPC
č
č
muon detector
Pb-Sc shower counters
NaI
magnet, drift chambers
4 5 6 7 8 9
9 8 7 6 5 4 3 2 1 0 1 2 3 4 5 6 7 8 9
Meters

Fig.3

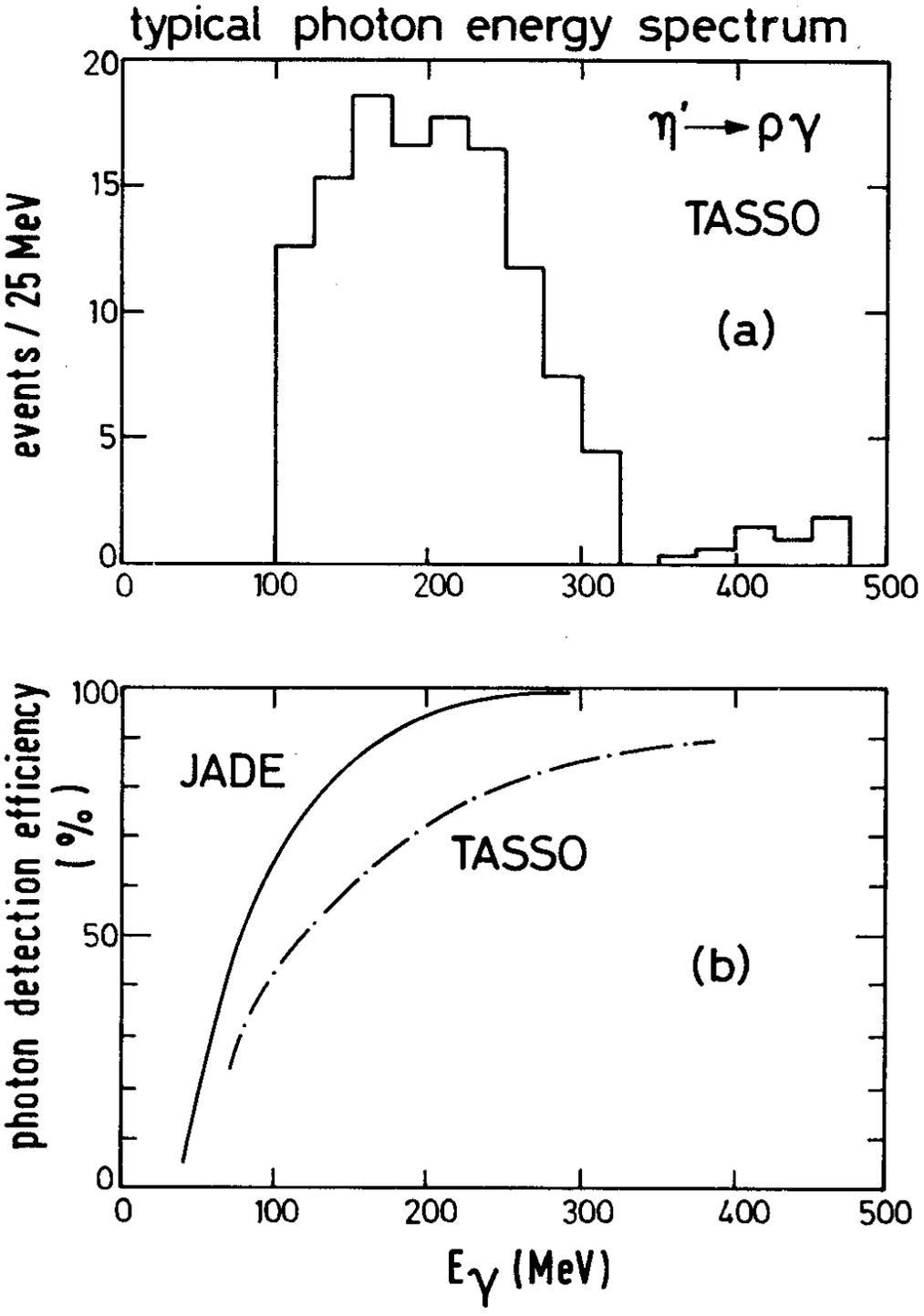
typical photon energy spectrum
events / 25 MeV
η' → ργ
TASSO
(a)
0
5
10
15
20
0
100
200
300
400
500
photon detection efficiency (%)
JADE
TASSO
(b)
0
50
100
0
100
200
300
400
500
Eγ (MeV)

Fig.4

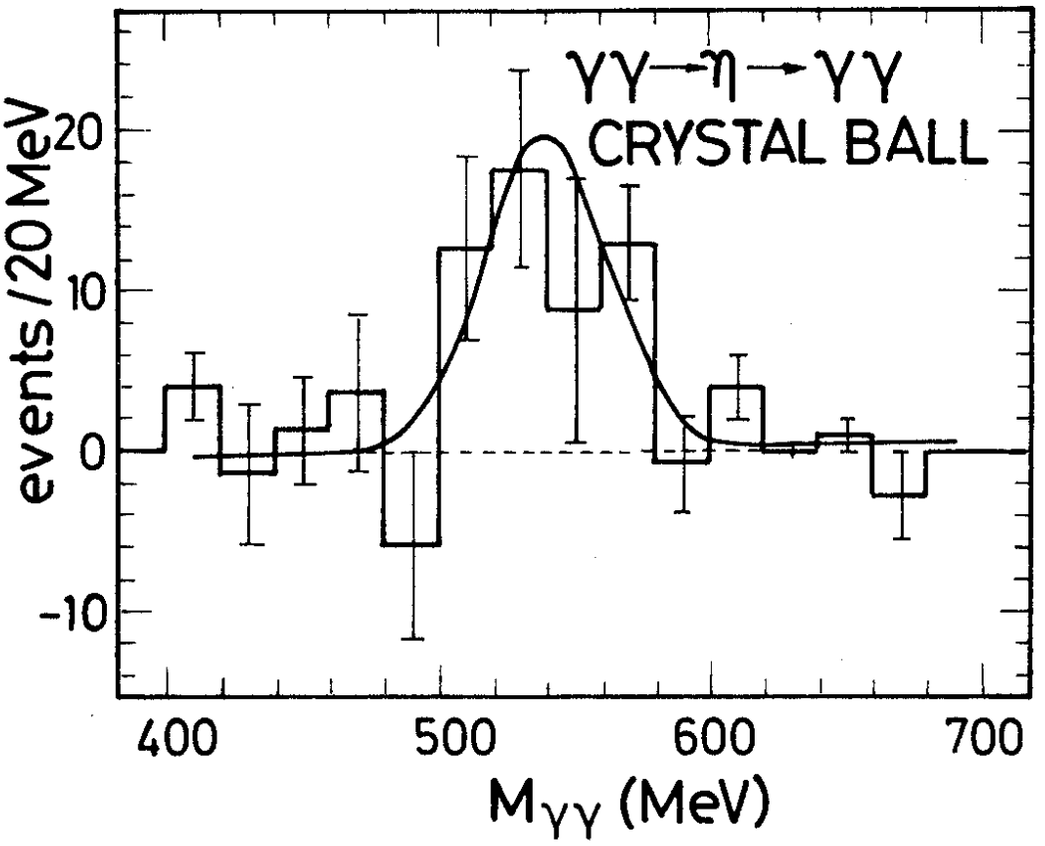
γγ→η→γγ
CRYSTAL BALL
events /20 MeV
20
10
0
-10
400
500
600
700
Mγγ (MeV)

Fig.5

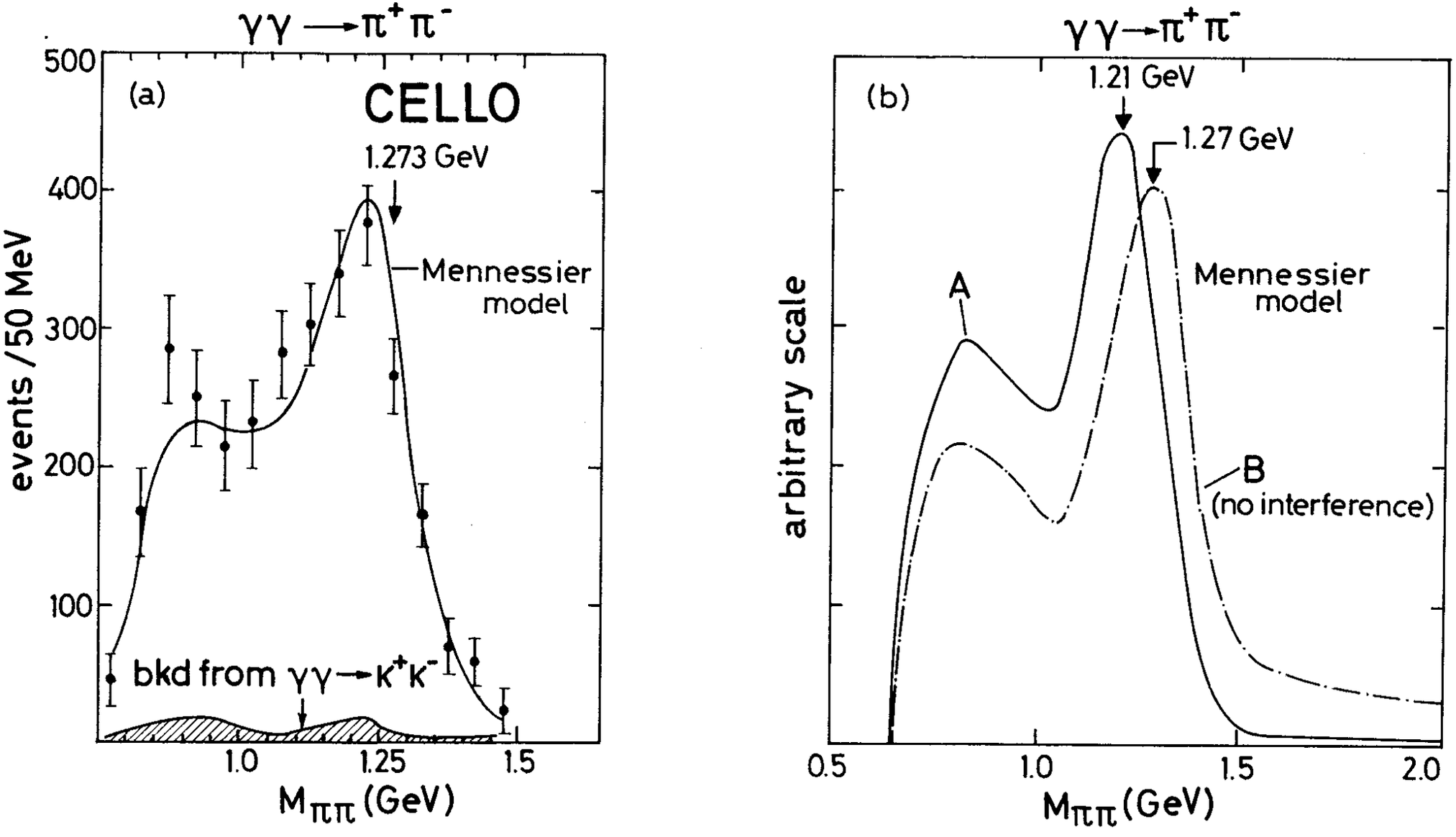
γγ → π⁺π⁻
(a)
CELLO
1.273 GeV
Mennessier model
bkd from γγ → K⁺K⁻
events /50 MeV
500
400
300
200
100
1.0
1.25
1.5
Mππ (GeV)
γγ → π⁺π⁻
(b)
1.21 GeV
1.27 GeV
A
Mennessier model
B
(no interference)
arbitrary scale
0.5
1.0
1.5
2.0
Mππ (GeV)

Fig.6

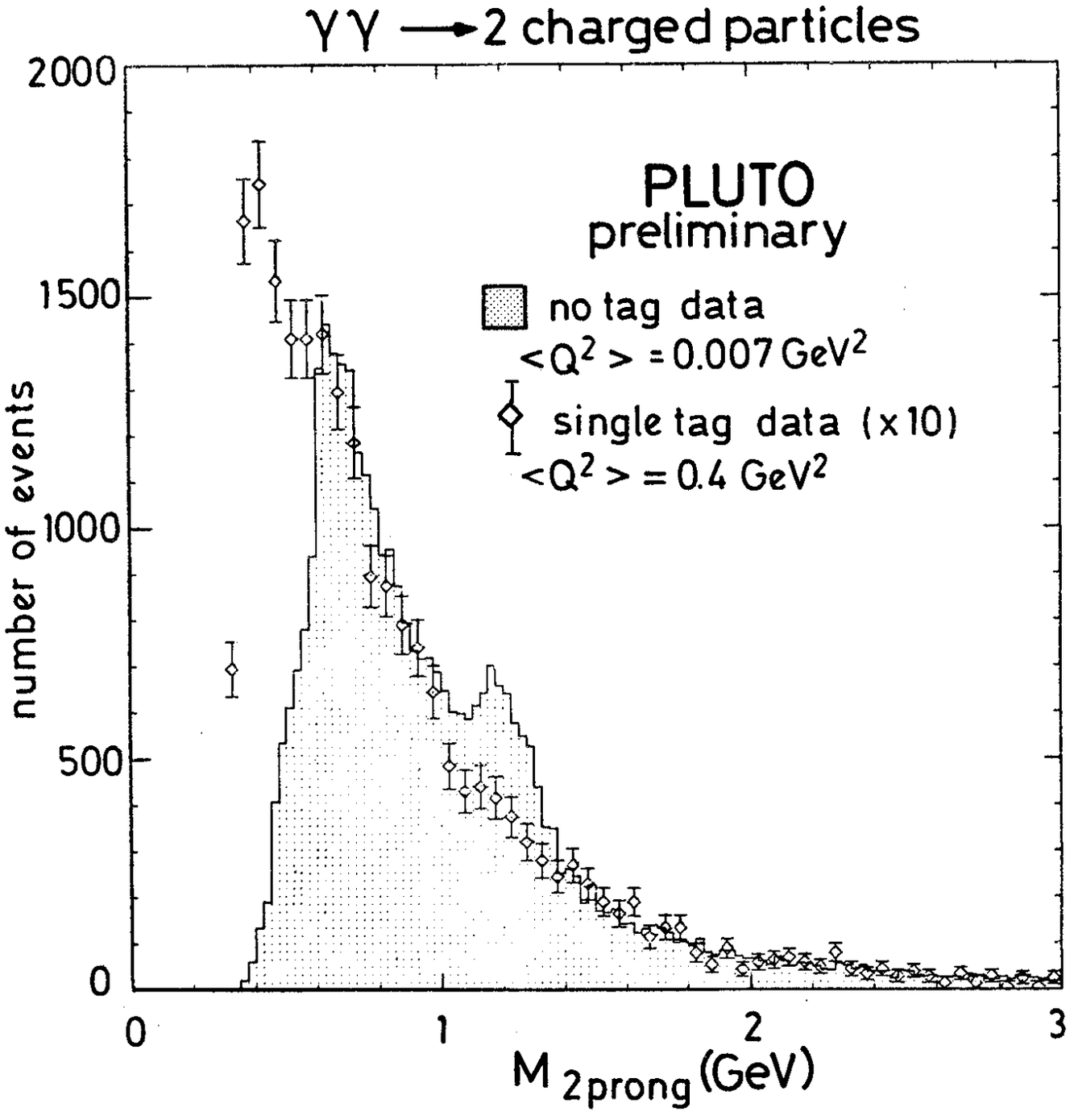
γγ ⟶ 2 charged particles
PLUTO
preliminary
no tag data
<Q² > = 0.007 GeV²
single tag data (x10)
<Q² > = 0.4 GeV²
number of events
2000
1500
1000
500
0
0
1
2
3
M 2prong (GeV)

Fig.7

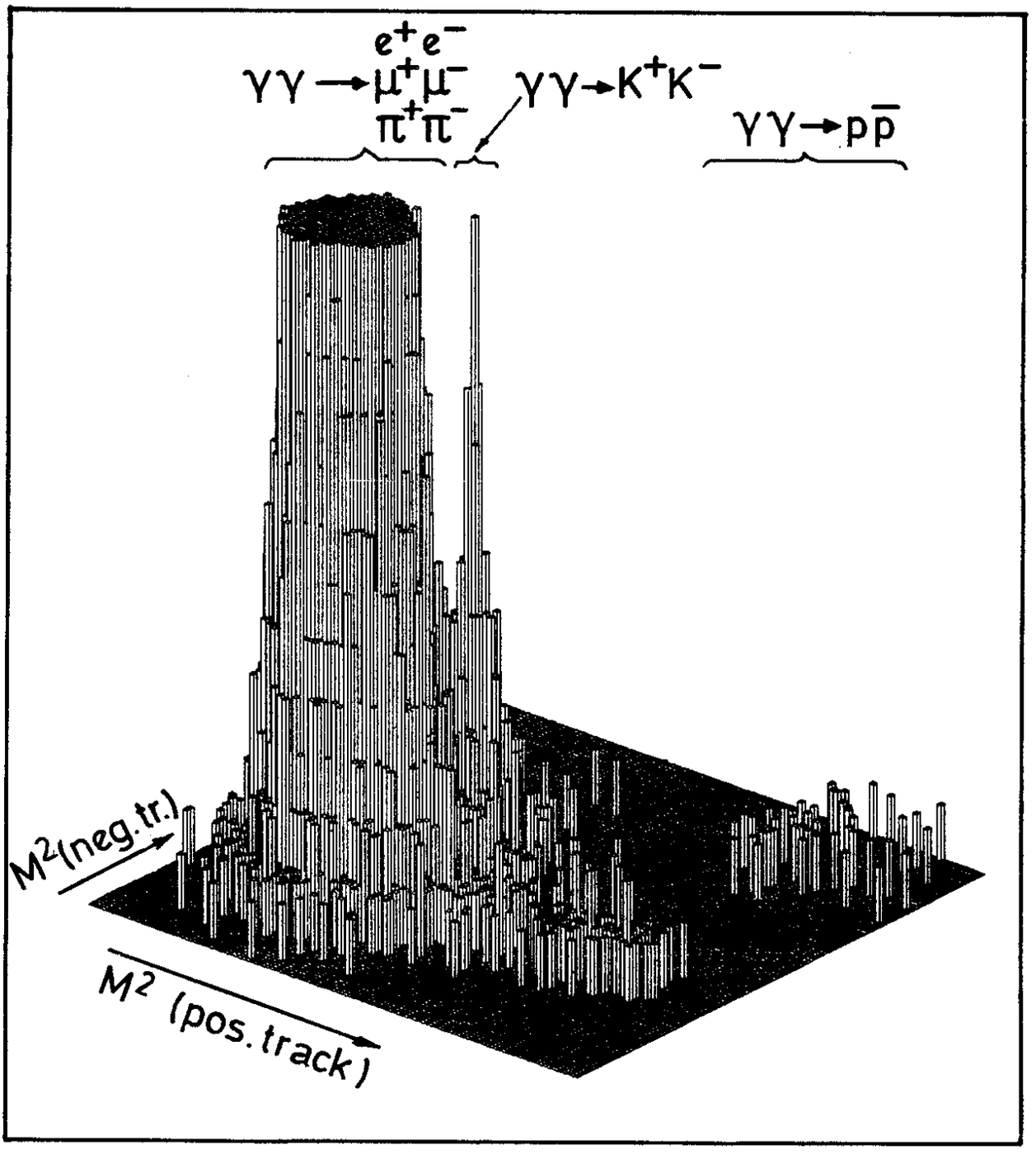
e^+e^-
$\gamma\gamma \rightarrow \mu^+\mu^-$
$\pi^+\pi^-$
$\gamma\gamma \rightarrow K^+K^-$
$\gamma\gamma \rightarrow p\bar{p}$
M^2(neg. tr.)
M^2 (pos. track)

Fig.8

Fig.9

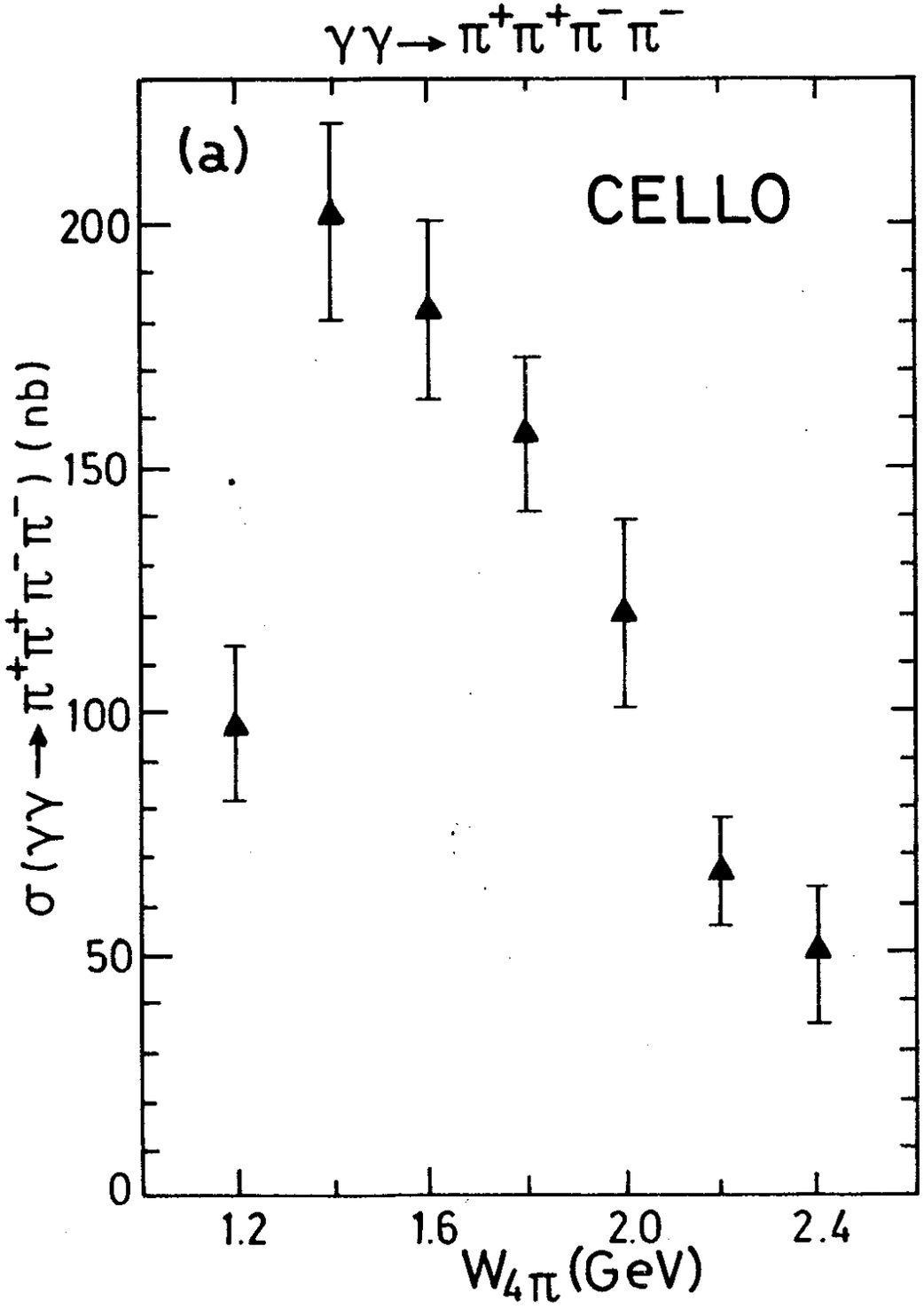
γγ → π⁺π⁺π⁻π⁻
(a)
CELLO
σ(γγ → π⁺π⁺π⁻π⁻) (nb)
200
150
100
50
0
1.2
1.6
2.0
2.4
W4π (GeV)

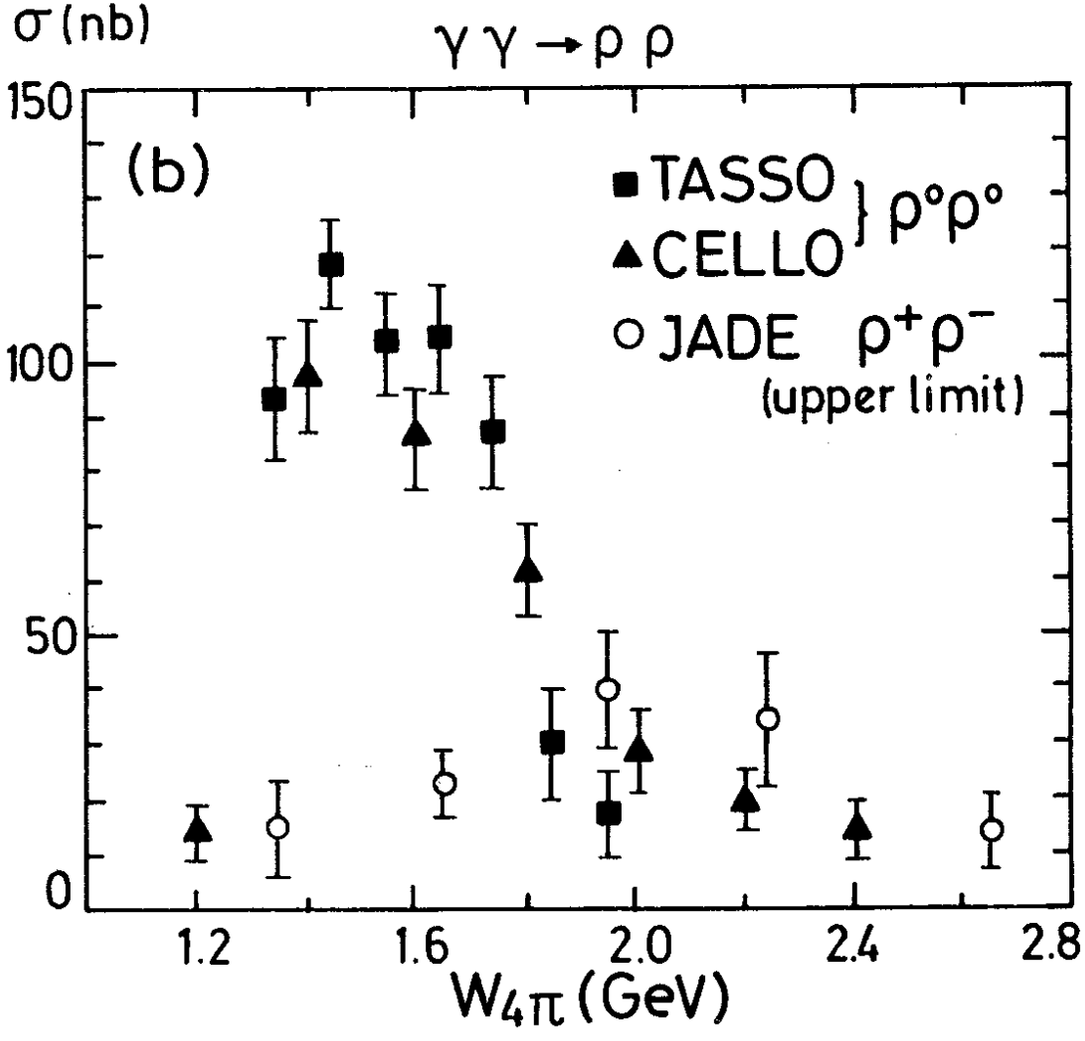
σ (nb)
γγ → ρρ
(b)
TASSO
CELLO
} ρ°ρ°
JADE ρ⁺ρ⁻
(upper limit)
150
100
50
0
1.2
1.6
2.0
2.4
2.8
W4π (GeV)

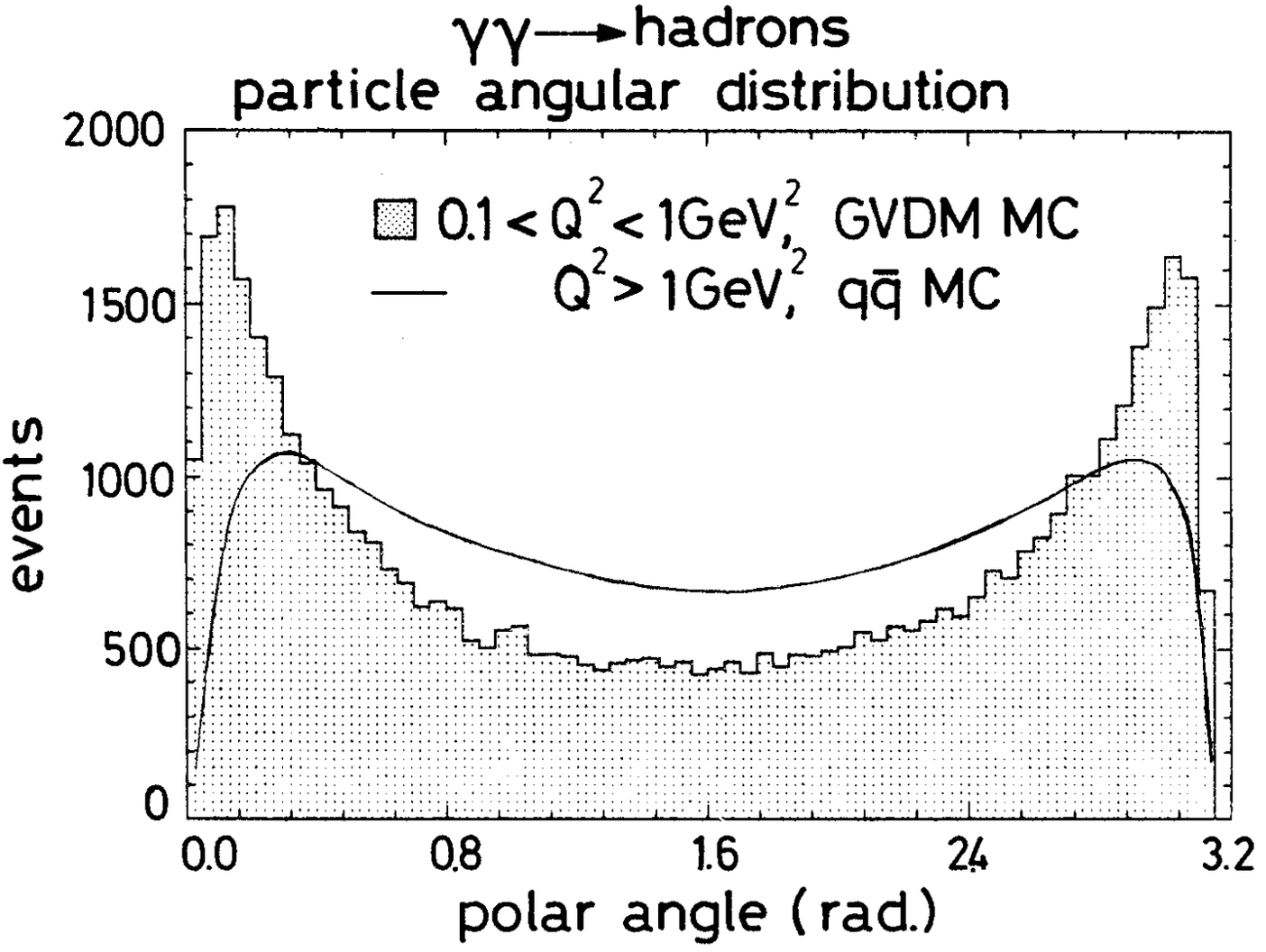
γγ⟶hadrons
particle angular distribution
0.1 < Q² < 1GeV², GVDM MC
Q² > 1GeV², qq̄ MC
events
2000
1500
1000
500
0
0.0
0.8
1.6
2.4
3.2
polar angle (rad.)

Fig.10

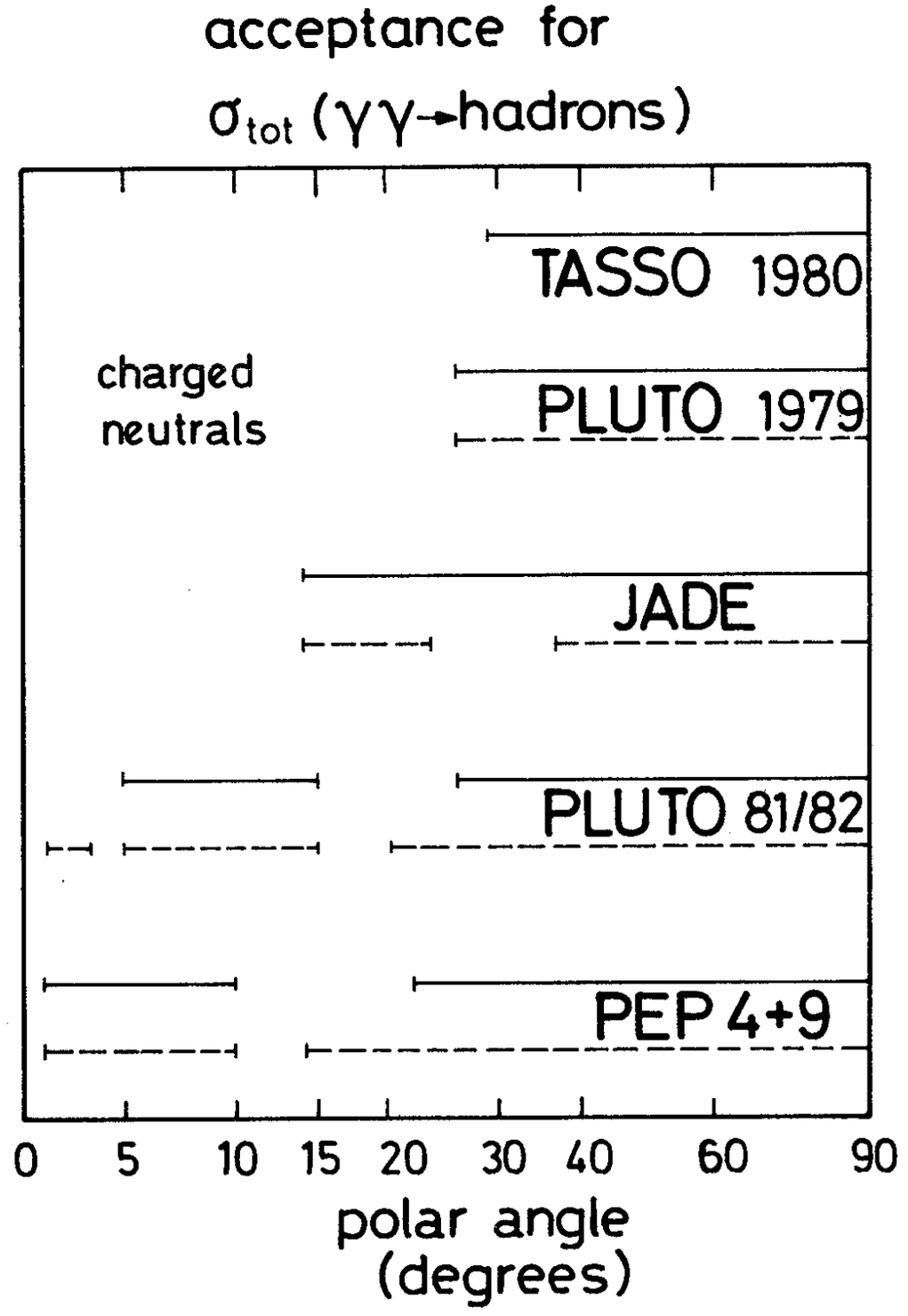
acceptance for
σtot (γγ→hadrons)
TASSO 1980
charged
neutrals
PLUTO 1979
JADE
PLUTO 81/82
PEP 4+9
0
5
10
15
20
30
40
60
90
polar angle
(degrees)

Fig.11

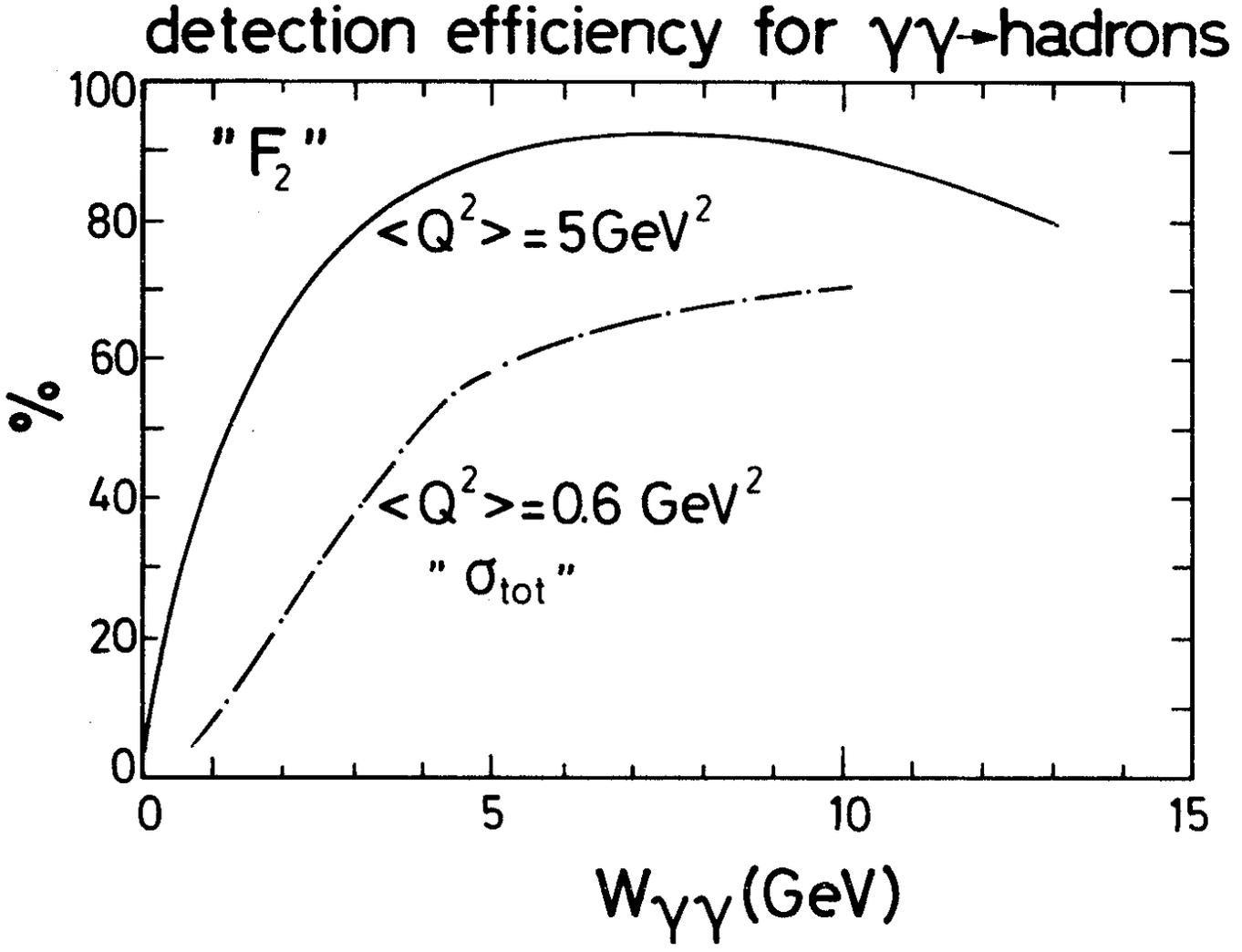
detection efficiency for γγ→hadrons
100
80
60
40
20
0
%
"F2"
<Q2>=5GeV2
<Q2>=0.6 GeV2
"σtot"
0
5
10
15
Wγγ(GeV)

Fig.12

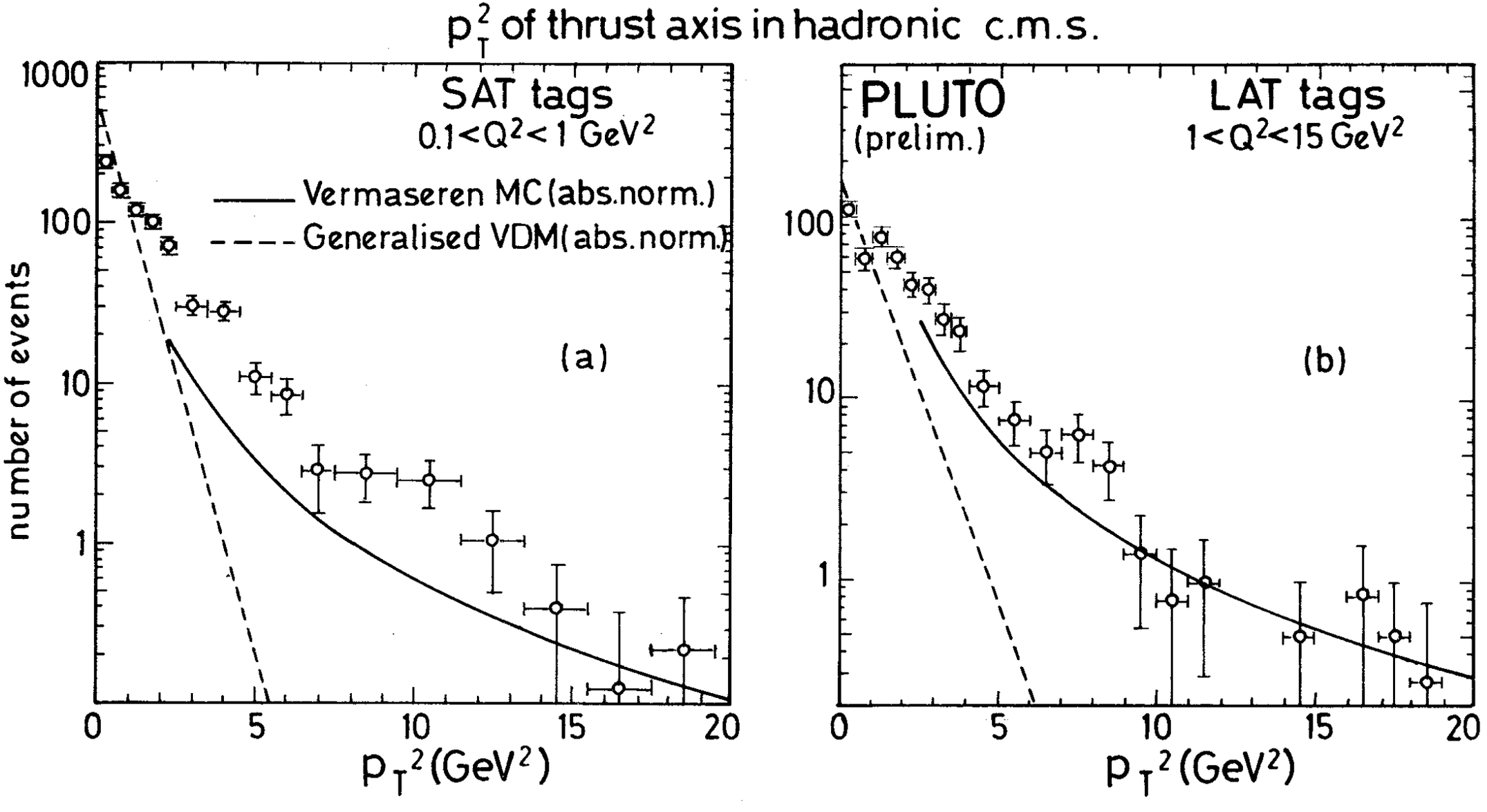
p_T^2 of thrust axis in hadronic c.m.s.
SAT tags
0.1<Q²<1 GeV²
Vermaseren MC (abs.norm.)
Generalised VDM (abs.norm.)
(a)
number of events
p_T^2 (GeV²)
PLUTO
(prelim.)
LAT tags
1<Q²<15 GeV²
(b)
p_T^2 (GeV²)

Fig.13

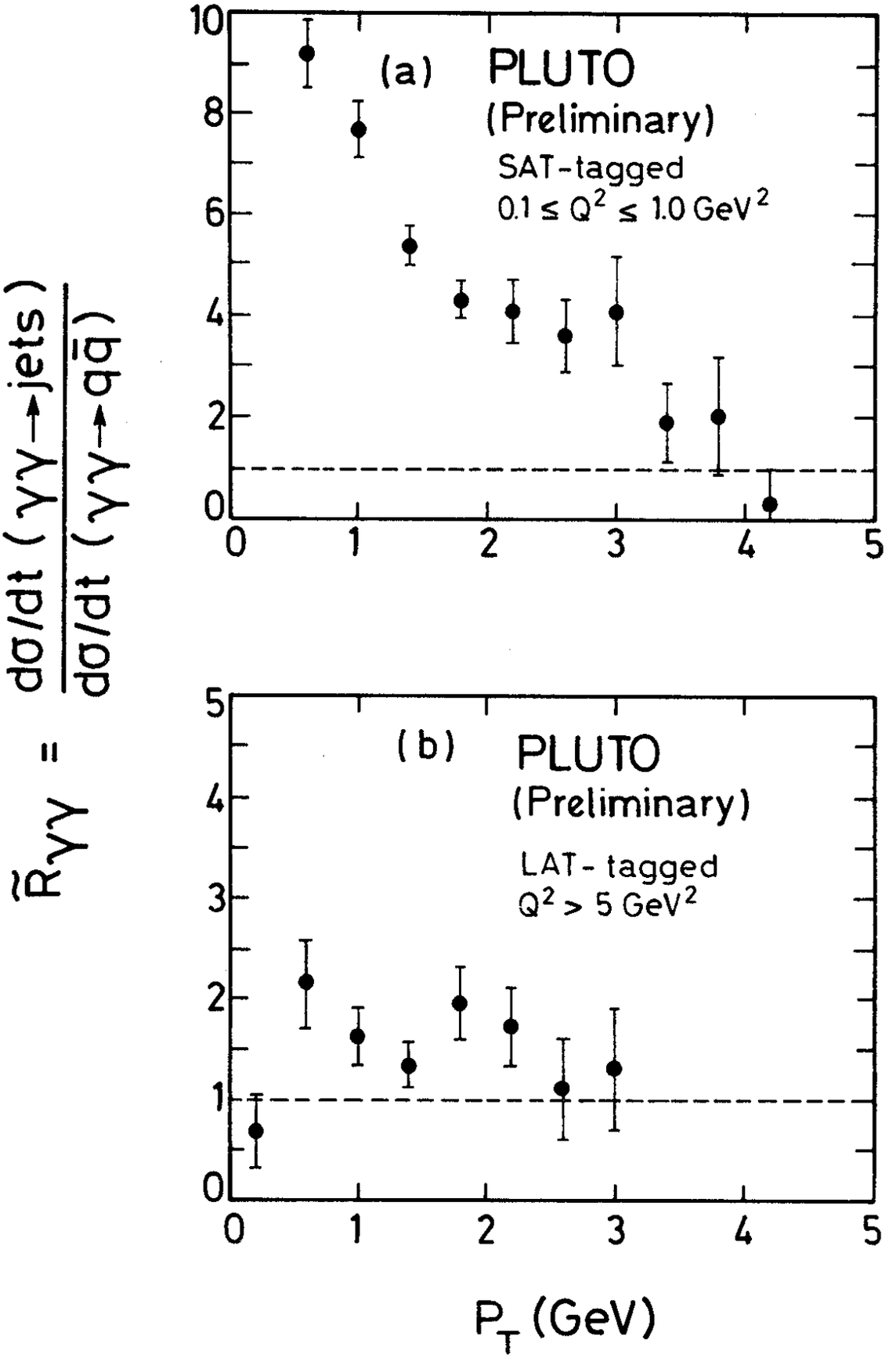
$\tilde{R}_{\gamma\gamma} = \frac{d\sigma/dt\,(\gamma\gamma \to \text{jets})}{d\sigma/dt\,(\gamma\gamma \to q\bar{q})}$
(a) PLUTO
(Preliminary)
SAT-tagged
$0.1 \leq Q^2 \leq 1.0\ \text{GeV}^2$
(b) PLUTO
(Preliminary)
LAT-tagged
$Q^2 > 5\ \text{GeV}^2$
P_T (GeV)

Fig.14

potential for structure function measurement

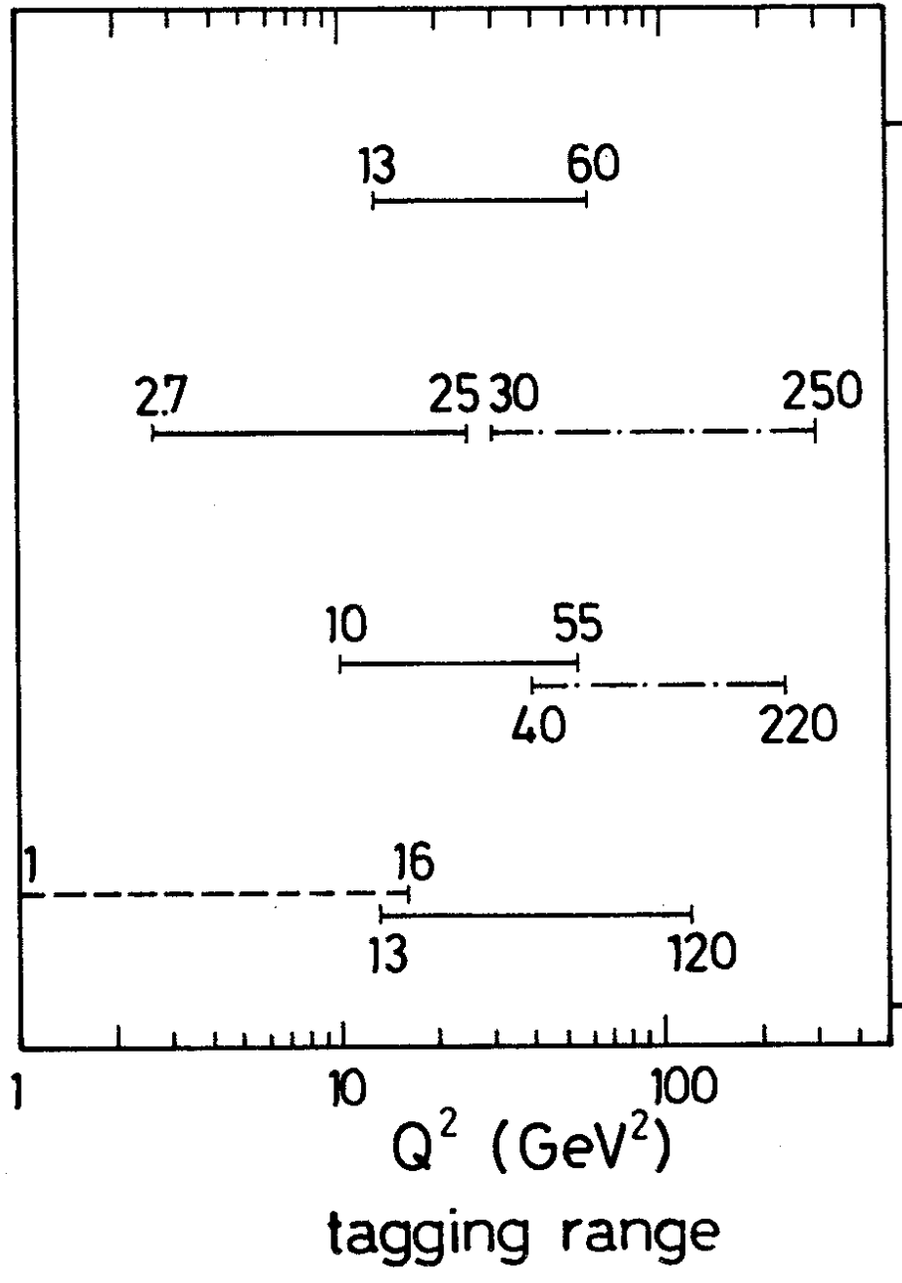

(b)

	# of events			antitagging
LAT	EC	BA	$\langle \frac{W_{vis}}{W} \rangle$	below 100 mr.
–	216	–	0,65	no
–	222	7	0,6	no
–	379	24	0,7	yes 43-78
1360	122	–	0,75/0,91	yes 30-60

Fig.15

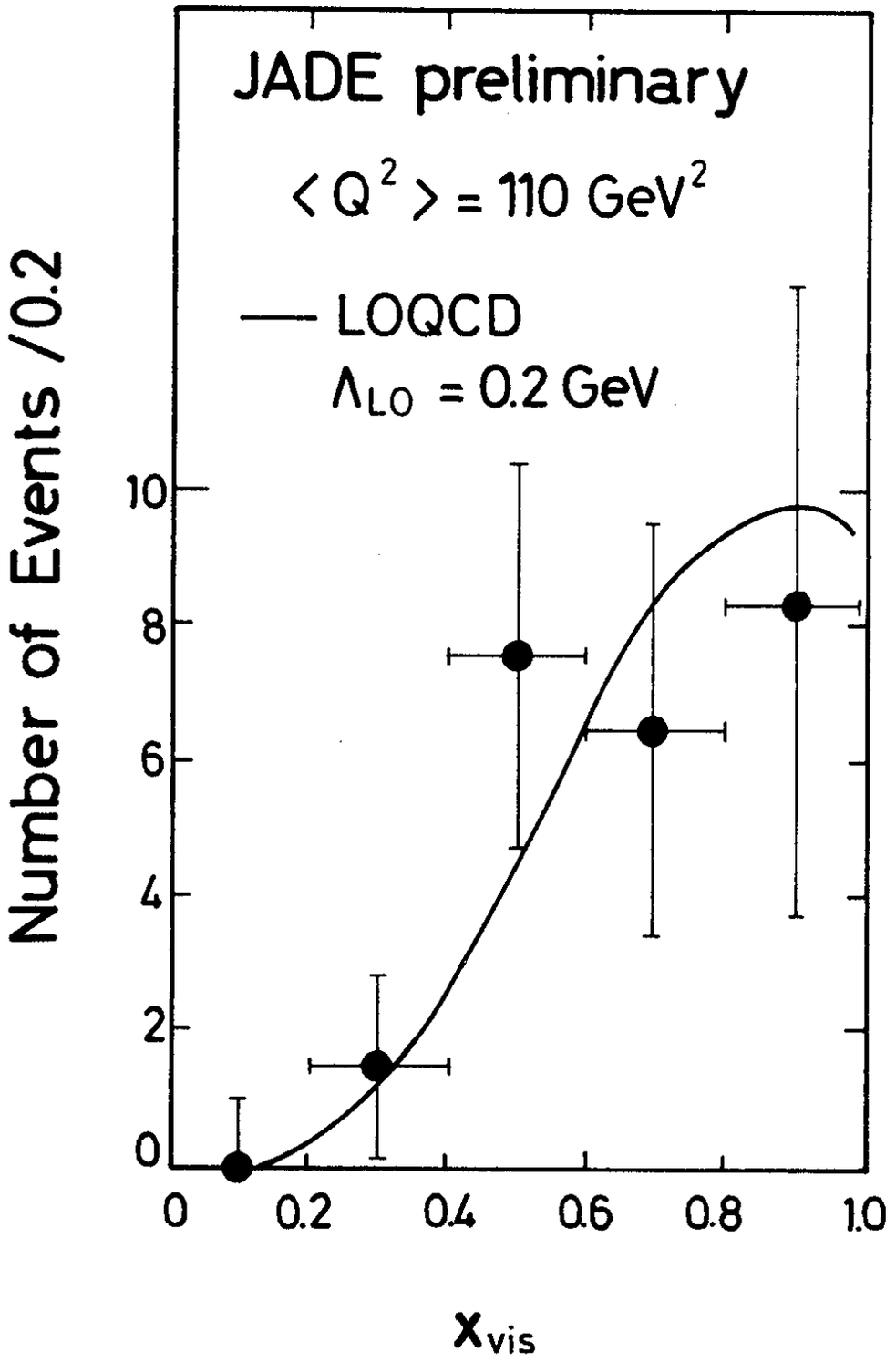
JADE preliminary
$\langle Q^2 \rangle$ = 110 GeV^2
— LOQCD
Λ_{LO} = 0.2 GeV
Number of Events /0.2
0
2
4
6
8
10
0
0.2
0.4
0.6
0.8
1.0
x_{vis}

Fig.16

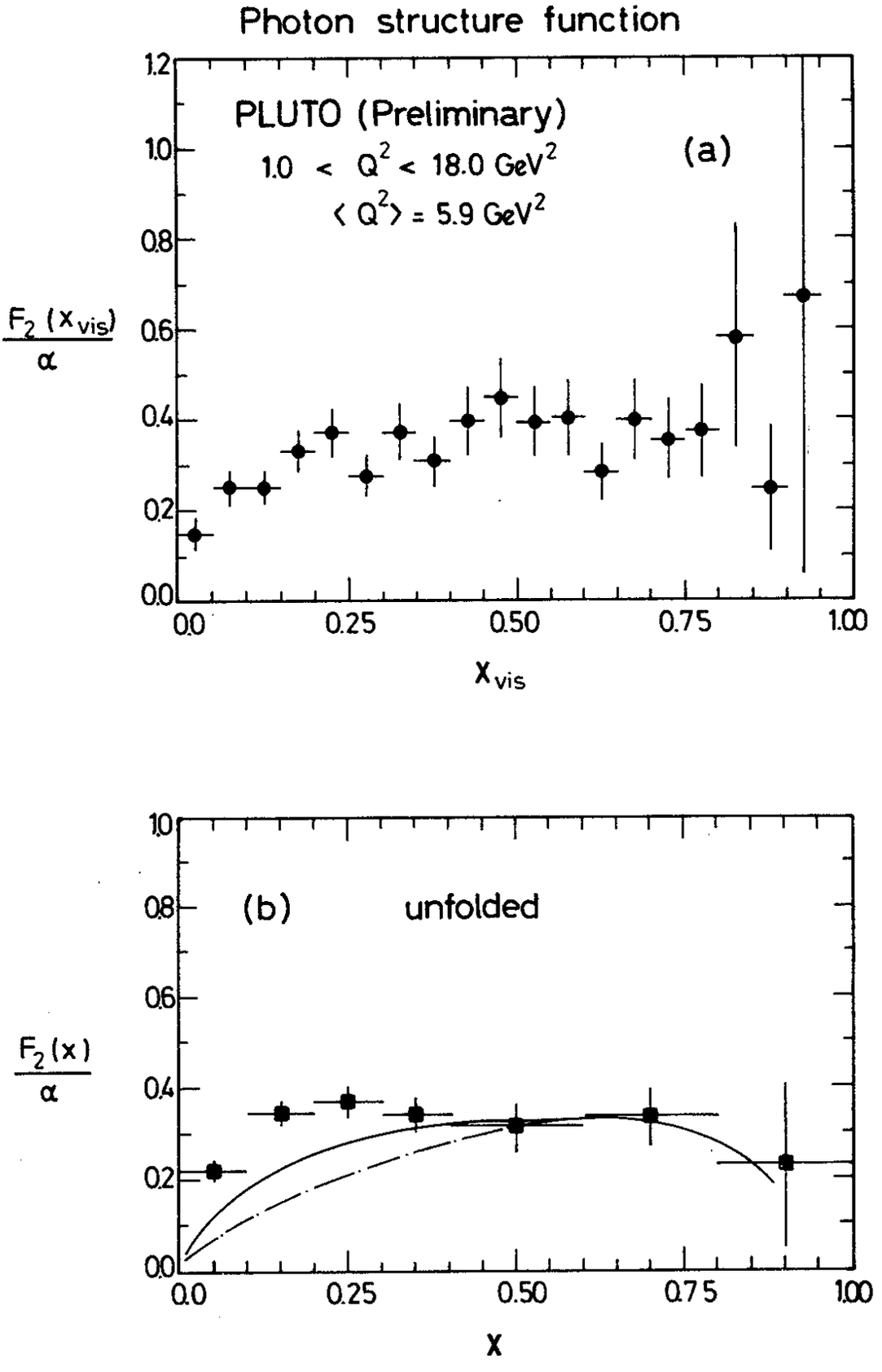
Photon structure function
PLUTO (Preliminary)
1.0 < Q² < 18.0 GeV²
⟨Q²⟩ = 5.9 GeV²
(a)
F₂ (x_vis) / α
x_vis
(b) unfolded
F₂(x) / α
x
0.0
0.25
0.50
0.75
1.00
0.2
0.4
0.6
0.8
1.0
1.2

Fig.17

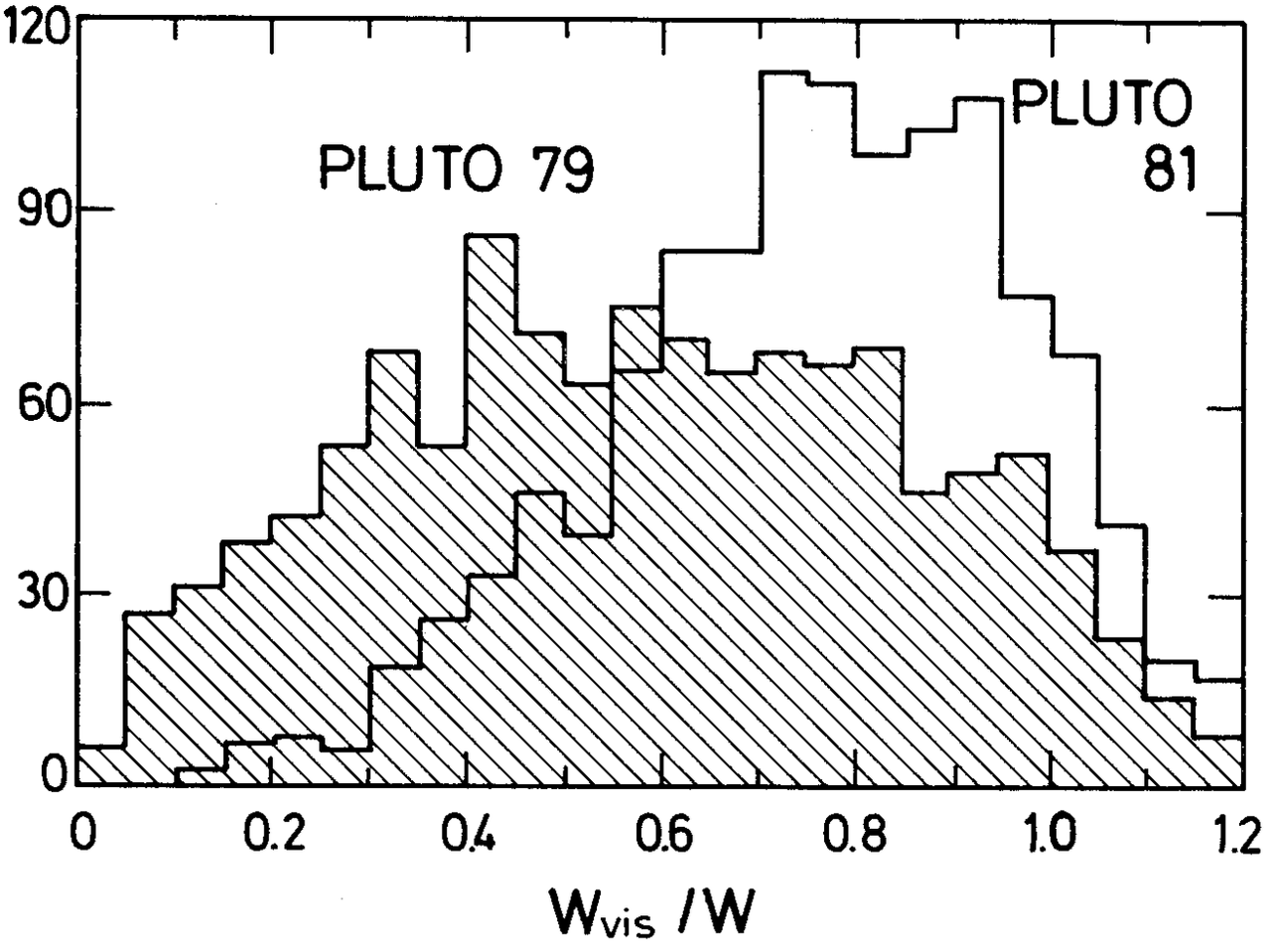

Fig.18

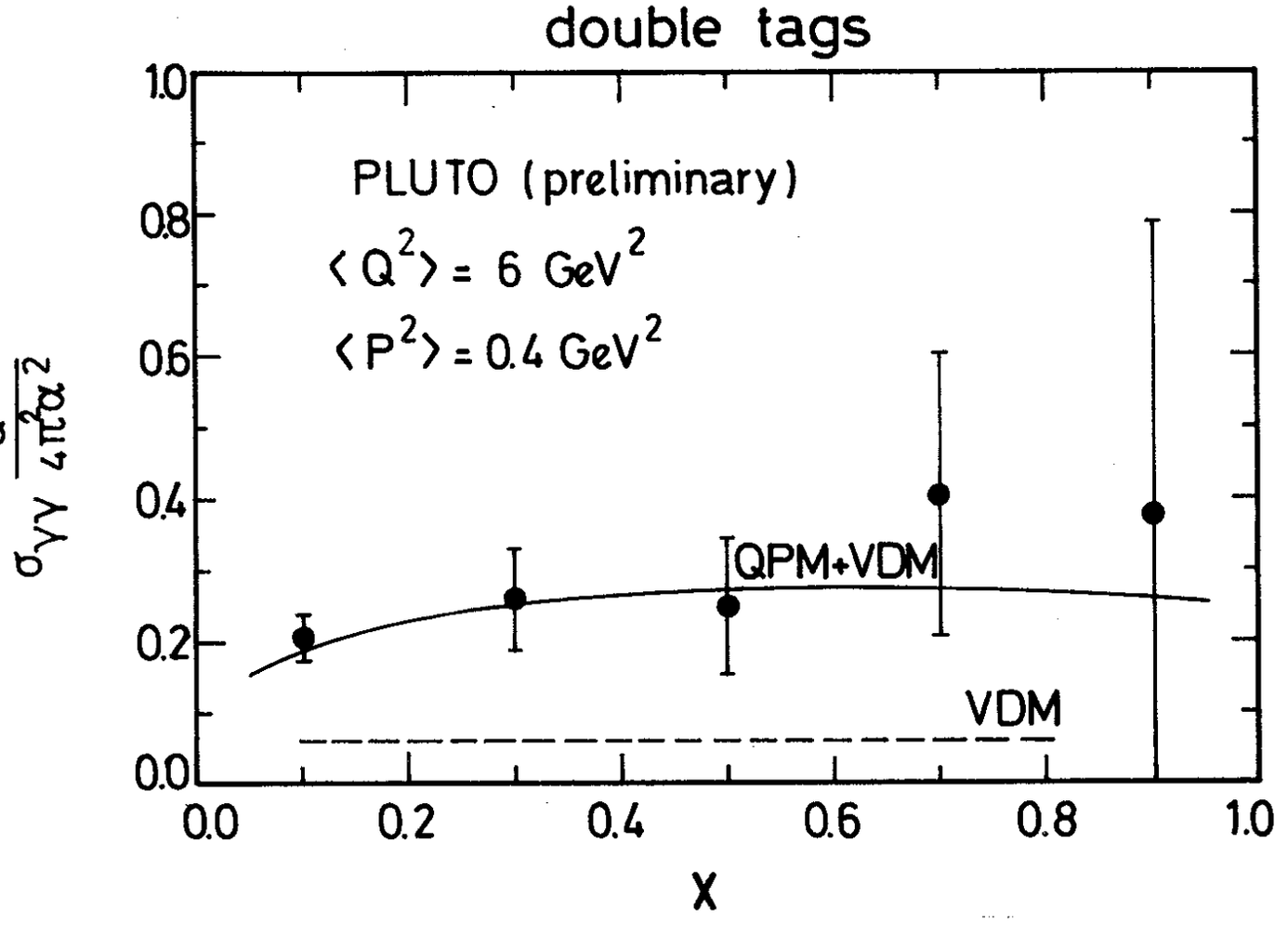
double tags
PLUTO (preliminary)
⟨Q²⟩ = 6 GeV²
⟨P²⟩ = 0.4 GeV²
QPM+VDM
VDM
$\frac{Q^2}{\sigma_{\gamma\gamma}\ 4\pi^2\alpha^2}$
X
0.0
0.2
0.4
0.6
0.8
1.0

Fig. 19